Characterization of the mean and extreme Mediterranean cyclones and their variability during the period 1500 BCE to 1850 CE

Onno Doensen[1,2], Martina Messmer[1,2,3], Woon Mi Kim[4,5], and Christoph C. Raible[1,2]

[1]Oeschger Centre for Climate Change Research, University of Bern, Bern, Switzerland
[2]Climate and Environmental Physics, University of Bern, Bern, Switzerland
[3]now at: Delft University of Technology, Civil Engineering and Geosciences, Geoscience and Remote Sensing, Delft, The Netherlands
[4]Climate and Global Dynamics Laboratory, NSF National Center for Atmospheric Research, Boulder CO, USA
[5]now at: Institute of Meteorology and Climate Research, Department of Tropospheric Research, Karlsruhe Institute of Technology, Karlsruhe, Germany

Correspondence: Onno Doensen (onno.doensen@unibe.ch)

Abstract. Extratropical cyclones are important meteorological phenomena in the Mediterranean and essential for local water supplies, yet they also pose significant hazards for the region as a result of extreme precipitation or wind events. Although they have been extensively studied using global and regional climate models, their spatial and temporal variability in the late Holocene is poorly understood. Here, we study a 3350-year climatological simulation that allows us to characterise Mediterranean cyclones better and provides a baseline for more accurately assessing the long-term effects of future climate change on Mediterranean cyclones. To analyse Mediterranean cyclone characteristics, we use a seamless transient simulation from 1500 BCE to 1850 CE produced by the Community Earth System Model with a 6-hourly temporal and $1.9° \times 2.5°$ horizontal resolutions. We found that Mediterranean cyclones exhibit pronounced multi-decadal variability in the order of 5% throughout the entire late Holocene with respect to several cyclone-related properties. For the cyclone frequency, a weak statistical relationship is identified with the East-Atlantic, the East-Atlantic Western-Russia, and the Scandinavian modes of circulation. ~~Cyclone frequency shows, although small, a significant increase in the eastern Mediterranean after severe volcanic eruptions with the highest sulphur injections. The composites~~ Composite analyses of the most extreme cyclones with respect to wind speed and precipitation indicate that cyclones in the central Mediterranean have the potential to grow more intense over their entire lifetime than cyclones in the eastern Mediterranean. This is especially true for extreme wind speed cyclones, implying that people in the central Mediterranean are potentially more exposed to hazards caused by extreme cyclones.

1 Introduction

The Mediterranean has long been recognized as one of the most active storm track regions in the world. Due to its uniquely complex topography, Mediterranean cyclones are generally smaller in scale, less intense, and of shorter life span than cyclones in other major storm track areas (Trigo, 2006; Flaounas et al., 2014). Yet, these cyclones can heavily impact the Mediterranean region as a result of heavy precipitation events (Pfahl and Wernli, 2012; Flaounas et al., 2015a; Raveh-Rubin and Wernli, 2015), heavy wind storms (Nissen et al., 2010; Raveh-Rubin and Wernli, 2015), and coastal floods (Lionello et al., 2019; Ferrarin

et al., 2021). These hazards can also occur simultaneously, resulting in compounding events that can have larger impacts than individual events combined (Zscheischler et al., 2018; Messmer and Simmonds, 2021; Vakrat and Hochman, 2023; Portal et al., 2024). Pfahl and Wernli (2012) showed that precipitation extremes and the presence of a cyclone are related up to 80% of the time in the Mediterranean, whereas Nissen et al. (2010) showed that the majority of wind extremes in the Mediterranean is caused by cyclones present in the Mediterranean. Portal et al. (2024) showed that compounding rain-wind and wind-wave extreme events in the Mediterranean are mostly caused by cyclones. Besides, Mediterranean cyclones are important for local water and energy supplies due to the precipitation they bring into this semi-arid region (Seager et al., 2014). However, the factors driving the variability of Mediterranean cyclone characteristics, especially extreme cyclones, are not fully understood. Thus, the purpose of this study is to deepen our understanding of Mediterranean cyclones by analysing past climate variability effects on the frequency and intensity of these types of cyclones using the Community Earth System Model (CESM; Hurrell et al., 2013).

Mediterranean cyclones occur more frequently in winter and have a frequency minimum in summer, with extreme cyclones being even less likely in summer (Flaounas et al., 2015b). The main cyclone hotspots in the Mediterranean are over the Gulf of Genoa, the Adriatic Sea, the Tyrrhenian Sea, the Aegean Sea, around Cyprus, and the Sahara (Lionello et al., 2016; Flaounas et al., 2018). However, processes governing cyclone formation are distinctly different for the different regions. Cyclones in the Gulf of Genoa and Adriatic Sea are mostly caused by lee processes related to the Alps associated with negative geopotential height anomalies over central and northern Europe (Trigo et al., 2002). Also, lee effects of the Atlas Mountains are the dominant cause of cyclogenesis over the Sahara in spring. Cyclones over the Aegean Sea are often caused by a large trough west of the area bringing vorticity to an area with warm sea surface temperatures (Trigo et al., 2002). Generally, the deepest cyclones can be found over the Gulf of Genoa and the Adriatic Sea, and cyclones over this region also tend to move slower than in other regions (Doiteau et al., 2024). Most Mediterranean cyclones originate in the Mediterranean basin, with only about 20% of cyclones developing over an area outside the Mediterranean (mainly the Atlantic) (Lionello et al., 2016). Still, extreme Mediterranean cyclones are most of the time dynamically associated with an ~~upstreams~~ upstream cyclone in the North Atlantic (Raveh-Rubin and Flaounas, 2017). Within the Mediterranean, several subtypes of cyclones are classified. The lee cyclones forming over the Gulf of Genoa and Adriatic Sea as discussed before, are called Genoa lows and are a well-known subtype. They can heavily impact weather over the Alps, southern France, and Italy (Mesinger and Strickler, 1982). Sometimes, these Genoa lows follow a track northeastwards into central Europe and are then classified as Vb-cyclones (van Bebber, 1891). These are quite rare events, but can heavily impact the Alps and central Europe as they often cause heavy precipitation (Mudelsee et al., 2004; Messmer et al., 2015; Krug et al., 2021; Stucki et al., 2020). The lee cyclones formed over the Sahara are called Sharav cyclone, and tend to rapidly travel eastwards. Due to their origin in arid areas, they often contain little moisture and can trigger dust storms over the Mediterranean (Alpert and Ziv, 1989). A special type of Mediterranean cyclone are so-called Medicanes, which are hybrid systems between tropical and extratropical storms and often occur in autumn and winter (Cavicchia et al., 2014). Medicanes have received lots of attention in recent years due to their intensity. However, due to their rarity, their overall socio-economic impact is not as large as that of extratropical Mediterranean cyclones (Flaounas et al., 2022).

In general, extratropical cyclone activity shows a distinct decadal variability (Feser et al., 2015). This variability can partly be explained by variations in different atmospheric modes of circulation (Seierstad et al., 2007; Walz et al., 2018). The most important mode of circulation influencing Mediterranean cyclones is the North Atlantic Oscillation (NAO). A positive NAO phase is statistically connected with a decrease in cyclone frequency over the Mediterranean, whereas an increase in cyclone frequency is found during the negative phase of the NAO (Raible et al., 2007). Moreover, the NAO is also inversely correlated to wintertime precipitation over the Mediterranean (Brandimarte et al., 2011; Montaldo and Sarigu, 2017). Hofstätter and Blöschl (2019) showed that clustering of Vb-cyclones becomes more frequent during negative NAO-phases. Other modes, like the East Atlantic (EA), Scandinavian (SCAN) and East Atlantic Western Russian (EAWR) and the Polar-Eurasian (POL) modes of variability, also have a significant influence on cyclones in the Northern Hemisphere (Seierstad et al., 2007). In addition to the modes of atmospheric circulation, Walz et al. (2018) hypothesized that sea ice anomalies are a dominant factor in the inter-annual variability of Mediterranean cyclones.

Besides natural influences, there is evidence that anthropogenic climate change has altered and is expected further to affect the frequency and intensity of Mediterranean cyclones. Winter precipitation in the Mediterranean declined during the 20th century, and one of the causes is a decrease in cyclogenesis in the region (Trigo et al., 2000). In addition to that, Nissen et al. (2014) suggested that NAO values may get more positive in the future, implying a northward shift of the jet stream, which will reduce cyclone activity in the Mediterranean. An increase in pressure, a decrease in baroclinicity, and an increase in static stability are further effects of climate change decreasing the number of cyclones in the Mediterranean (Hochman et al., 2020; Raible et al., 2010).

General circulation models (GCM) are extensively used to analyse the future impact of climate change and have also been extensively used to analyse Mediterranean cyclones and their future changes (Raible et al., 2010; Nissen et al., 2014). However, GCMs often have systematic biases related to extratropical cyclone frequency and intensity because of the low horizontal resolution and biases in land and sea surface temperatures (Zappa et al., 2013; Priestley et al., 2023). Mediterranean cyclones, which are usually of a smaller spatial scale than other extratropical cyclones, suffer even more from the low resolution in GCMs (Flaounas et al., 2013). Moreover, the relatively short period that simulations from GCMs cover makes analyses of the long-term variability of extreme cyclones more uncertain (Raible et al., 2018). Hence, large uncertainties remain for future projections concerning extreme Mediterranean cyclones.

An alternative method is to look at proxies to reconstruct the climate of the past (Xoplaki et al., 2003). Yet, since proxies are usually only sensitive to temperature and precipitation, and not to wind and pressure, it is complicated to reconstruct cyclone activity directly (Raible et al., 2021). Cyclone-related proxies often have to be derived from alterations in dust transport (Jong et al., 2006) or changes in sea sediment depositions (Degeai et al., 2015; Pouzet and Maanan, 2020). Still, some proxy-based records show that periods with more and less storm activity alternate during the Holocene (Degeai et al., 2015; Sabatier et al., 2012). Alternatively, reconstructions of the NAO can be used as an indirect measure of cyclone activity (Pinto and Raible, 2012; Ortega et al., 2015).

To overcome these problems, paleoclimate modelling that simulates much longer time periods than most simulations generally do is used (Raible et al., 2021). Thereby, GCMs attempt to reproduce past climates by considering natural and external

forcings and boundary conditions. The resulting simulations of the past climate can be verified by comparing them against proxies (2k PMIP3 group, 2015; PAGES Hydro2k Consortium, 2017). Simulations of the past climate are also used to evaluate the ability of GCMs to represent internal climate variability, as well as creating a climatological baseline for specific events (Harrison et al., 2015; Kageyama et al., 2018). Several studies investigated the effect of climate variability during the Holocene on extratropical cyclones in the Northern Hemisphere (Raible et al., 2021; Varma et al., 2012; Xia et al., 2016), or on a synoptic scale in the Euro-Atlantic domain using GCMs (Raible et al., 2018). Raible et al. (2018) simulated the period between 850 CE and 2100 CE and showed that cyclones in the North Atlantic exhibit pronounced multi-decadal variations caused by internal variability of the climate system. A similar finding was also reported by Gagen et al. (2016) for summer extratropical cyclones in the North Atlantic. Regarding natural forcing, Andreasen et al. (2024) suggested that strong volcanic eruptions may increase the number of cyclones in the subtropics and high latitudes, whereas the number of cyclones in the midlatitudes decreases. However, earlier work by Fischer-Bruns et al. (2005) found no relation between differences in volcanic forcing and storm activity, and thus the effect of volcanic eruptions on cyclones remains uncertain.

In this study, we use the CESM to investigate the effects of past climate variability on the frequency and intensity of Mediterranean cyclones. The CESM simulation consists of a single-member transient run that covers the period from 1500 BCE until 2012 CE (3512 years in total) (Kim et al., 2021). We track all cyclones in the Mediterranean and its immediate surroundings until 1850 CE. We particularly focus on extreme Mediterranean cyclones for precipitation and wind speed. This approach aids in assessing and understanding the underlying processes that affect (extreme) Mediterranean cyclones and making better projections for the future.

The paper is organized as follows: In Sect. 2, we introduce the CESM simulation and tracking algorithm for Mediterranean cyclones in more detail. In Sect. 3, we evaluate the CESM simulations, show the internal climate variability and the relation between atmospheric modes of circulation related to extratropical cyclones and study the impact of volcanic eruptions on and extratropical cyclones. In Sect. 4 we show typical cyclone characteristics for different extremes for the central and eastern Mediterranean produced by CESM. Finally, in Sect. 5, we discuss the impacts of our results in a wider framework.

2 Methods and Data

2.1 General circulation model and reanalysis data

The CESM version 1.2.2 is a fully coupled global climate model consisting of various component models. We used a configuration with a horizontal resolution of $1.9°$(latitude) $\times$ $2.5°$ (longitude) in the atmosphere and over land and with a nominal $1.0° \times 1.0°$ resolution for the ocean and sea ice. The atmospheric component contains 30 vertical sigma pressure levels, and the ocean has 60 unevenly distributed layers. We used a seamless simulation spanning from 1500 BCE to 2012 CE with a 6-hourly temporal resolution, branched off a spin-up equilibrated simulation with 1501 BCE conditions (Kim et al., 2021). The simulation was forced by solar irradiance, greenhouse gas (GHG) concentrations, albedo changes, and volcanic sulphur injections into the stratosphere that covers the entire simulation period(Fig. ??a). . Most of the forcings were obtained from the Paleoclimate Modelling Intercomparison Project phase 4 (PMIP4) database, and the volcanic forcing was from Sigl et al.

(2021) and Carn et al. (2016). How these forcings were obtained and generated are explained in detail in Kim et al. (2021).

125   In this study, we used geopotential height at 1000 hPa (Z1000) and 500 hPa (Z500), sea level pressure (SLP), 850 hPa temperature anomaly (T850), total precipitation, which is the sum of the large-scale and convective precipitation, and horizontal wind components at 850 hPa and 300 hPa in the x- and y-direction, which are combined to wind speeds WS850 and WS300, respectively.
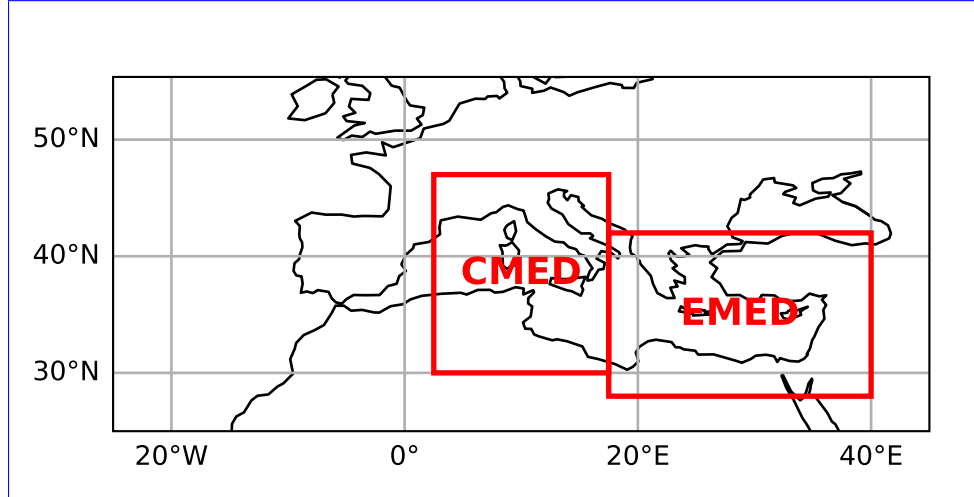
Figure 1. ~~(a) Overview of stratospheric sulphur injections into the stratosphere as a result of volcanic eruptions.~~ The ~~arrows indicate when the 20 eruptions with the highest sulphur injections occurred. (b) The~~ two regions of interest that are shown: "CMED" indicates the region defined as the central Mediterranean (between 2.5° E - 17.5° E and 30° N - 47° N), "EMED" indicates the region defined as the eastern Mediterranean (between 17.5° E - 40° E and 28° N - 42° N).

    To evaluate the representation of Mediterranean cyclones in CESM, we compared the CESM output with the ERA5 reanal-

130   ysis (Hersbach et al., 2020) for a period where both datasets overlap in time (1981–2010). ERA5 was regridded to the same spatial resolution as CESM to provide a fair comparison between the two.

2.2   Cyclone detection and tracking algorithm

We applied the cyclone detection and tracking algorithm developed by Blender et al. (1997) and extended by Schneidereit et al. (2010) to the seamless model simulation and ERA5 data. The algorithm identified minima in the Z1000 field. To exclude weak

135   and unrealistic low-pressure systems, the cyclones need to fulfil the following requirements:

    – A minimum mean gradient of at least 20 geopotential meters (gpm) per 1000 km is achieved.

    – During the whole cyclone's lifetime, a minimum mean gradient of 30 gpm per 1000 km is achieved at least once.

    – Local minima over grid cells with an orography higher than 1000 m above sea level are excluded.

- To connect different minima to a cyclone track, a minimum in the following time step is identified with a next-neighbour search. The new minimum of the cyclone must be within 250 km of the previous cyclone minimum.

- The minimal lifetime of a cyclone is at least 24 h.

The cyclone identification and tracking method provided a variety of cyclone characteristics, such as the cyclone position, the radius of a cyclone, the cyclone depth, the core (central) pressure, and cyclone-related mean and extreme precipitation and wind speed. To compute the cyclone radius, first, a Gaussian function was fitted to the Z1000 field, assuming that the cyclone was azimuthally symmetric (Schneidereit et al., 2010). The cyclone radius is then defined as the distance between the cyclone centre and the point of 1.5 standard deviation (which represents the middle between the first and second inflection points), as done by Messmer and Simmonds (2021). The depth of the cyclone is defined as the difference between Z1000 in the centre of the cyclone and the Z1000 mean over the area of 1000×1000 km^2.

To calculate the cyclone-related wind speed and precipitation, the maximum value of wind speed and precipitation of all grid cells within a cyclone's radius were considered (Raible et al., 2018). We also applied the tracking algorithm to the ERA5 Z1000 field to evaluate the Mediterranean cyclone characteristics in CESM, mostly focusing on the cyclone tracks.

2.3 ~~Superposed epoch analysis~~

~~To test the potential impact of volcanic eruptions on the frequency of Mediterranean cyclones, we applied the superposed epoch analysis to the simulation by analysing the mean conditions before and after the 20 strongest eruptions in the simulation (Lehner et al., 2015; Raible et al., 2018). These eruptions occurred over the whole globe, however most occurred in the tropics (16 out of 20). We considered the conditions of five years before an eruption occurs to be the baseline and compared the conditions of two years after the eruption as the perturbed comparison state. If two or more eruptions occurred within seven years of each other, we used the first five unperturbed years occurring before these eruptions as the unperturbed state and the two years after the last eruption as the perturbed state. To identify whether the cyclone frequency in the period after the eruption is significantly different to before the eruption, we apply a Welch's t-test (Welch, 1947) using 5% significance level.~~

2.3 Atmospheric modes of circulation and Mediterranean cyclones

To find the relation between atmospheric modes of circulation and Mediterranean cyclones, we first computed the most dominant modes of circulation over the North Atlantic domain in the CESM simulation. We applied an empirical orthogonal function (EOF) analysis to anomalies of Z500. For that, a 100-year period was selected from the simulation to compute the most important modes on seasonal time scales, and then these modes were projected on the rest of the monthly Z500 data for the whole simulation until 1850 CE. The EOF analysis was calculated for the region between 90° W - 40° E and 20° N - 80° N, similar to Hurrell (1995) (see Fig. S1). Finally, the principal components (PCs) of the EOFs were computed and normalized. To identify a relation between atmospheric modes of circulation and Mediterranean cyclones, the Pearson correlation coefficients were estimated between the PCs and the monthly cyclone frequency, cyclone-related precipitation and cyclone-related wind speed.

170 We only considered grid cells where the model orography is below 1000 m and where a cyclone frequency was higher than 0.01 day^{-1}.

2.4 Area of interest and analysis of extreme Mediterranean cyclones

Mediterranean cyclones are subject to large temporal and spatial variability (Campins et al., 2011). Therefore, we split the Mediterranean region into the central and the eastern Mediterranean (Fig. ??b1) and analysed extreme cyclones for each of
175 these regions. We exclude the western Mediterranean Sea and the Iberian Peninsula, as there were only a very limited number of grid points available for this region due to the rather coarse resolution of CESM, and based on our own analysis the western Mediterranean is heavily influenced by the Atlantic, and therefore the dominant processes here are not so relevant for the rest of the Mediterranean.

 To analyse extreme cyclones, we need to select the most extreme cyclones within the tail of their probabilistic distribution.
180 To do this, we ranked them based on WS850 (hereafter just wind speed) at the time when the cyclone reaches the lowest core sea level pressure within its track (hereafter $t0$) (similar to Pfahl and Sprenger (2016)), and based on the maximum 6-hourly cyclone-related precipitation (hereafter just precipitation) within the entire track that affects the region. The location of minimum pressure is obtained while the cyclone track stays within the respective region of interest, which is either the central or the eastern Mediterranean (Fig. ??b1), but the track can start and end outside the corresponding region. We estimated the
185 distributions of wind speed at $t0$ and of precipitation at the time step of maximum 6-hourly cyclone-related precipitation for all cyclones within the corresponding region. The distribution for precipitation is skewed towards extreme values and values close to zero. Therefore, all precipitation rates below 1mm mm (6h^{-1})$^{-1}$ were excluded, and we computed the square root of the remaining precipitation to approximate a Gaussian distribution for precipitation. Compound extreme precipitation and extreme wind events related to cyclones were defined with the joint probability distribution of the precipitation and wind speed
190 of all cyclones. Next, all the cyclones were ranked in terms of extremeness based on these distributions. We selected the 10, 100, and 1000 most extreme cyclones (hereafter EXC10, EXC100, EXC1000, EXC is used for extreme cyclones in general) for the central (out of 239476 in total) and eastern (out of 161768 in total) Mediterranean with respect to precipitation, wind speed, and compound events.

 Finally, a composite analysis was performed on the EXC10, EXC100, and EXC1000 to investigate the spatial and temporal
195 characteristics of cyclones associated with an extreme event. The following steps are carried out:

1. For each cyclone track, we set the reference at time $t0$. Every time step of the track that occurred after $t0$ obtains a positive index, and the time steps of the track that occurred before $t0$ receive a negative index.

2. For each of the 6-hourly time steps of the cyclone's track, all fields have been centred at the location of the cyclones, given by its core minimum pressure. With this approach, the model data for each cyclone track point was indepen-
200 dent of its geographical location. Since all the cyclones were located in the Mediterranean basin at $t0$ and, therefore, within a relatively small range of latitudes, variations due to differences in latitude weights of grid cells were considered insignificant and, therefore, negligible.

3. We were only interested in the 30 hours (5-time steps) before and after $t0$ for each cyclone to capture the intensification and decaying phase of the cyclone.

205 4. For every time step within these 30 hours before and after $t0$, we compute spatial averages for EXC10, EXC100, and EXC1000. This was done for both regions for cyclones associated with cyclone-related precipitation, wind, and compound extremes. Cyclone tracks that did not appear at any of these time steps were ignored for the temporal means.

The composite analysis was applied to the precipitation, wind speed, WS300, SLP, T850, Z500 and the Rossby wave packet (RWP) amplitude. The computation of the RWP amplitude is based on the method provided by Fragkoulidis et al. (2018) and
210 is produced by calculating the amplitude of the envelope of the 300 hPa meridional wind. A Welch's t-test was applied to all the temporal means and the spatial means of precipitation and wind speed between the two regions to assess whether EXCs between the two regions are significantly different.

3 Cyclone variability in the late Holocene

3.1 Evaluation of the CESM simulation against ERA5

215 In Fig. 2, we show the cyclone frequency for the period 1981–2010 in CESM and ERA5. Considering Europe and the North Atlantic, CESM reproduces the general storm tracks stretching from Newfoundland, via Iceland towards Scandinavia. However, CESM overestimates cyclone frequency over the polar North Atlantic and underestimates cyclone frequency in the subtropical North Atlantic. This bias is present in all seasons, but is particularly present during DJF (Fig. 2f), with differences up to 50%. Thus, the biases generally indicate that the simulated storm ~~track~~ tracks in the North Atlantic ~~is too zonal and shifted northward~~
220 ~~compared to the storm track in ERA5~~have a northward bias, and are to a lesser extent too zonal, especially in DJF.
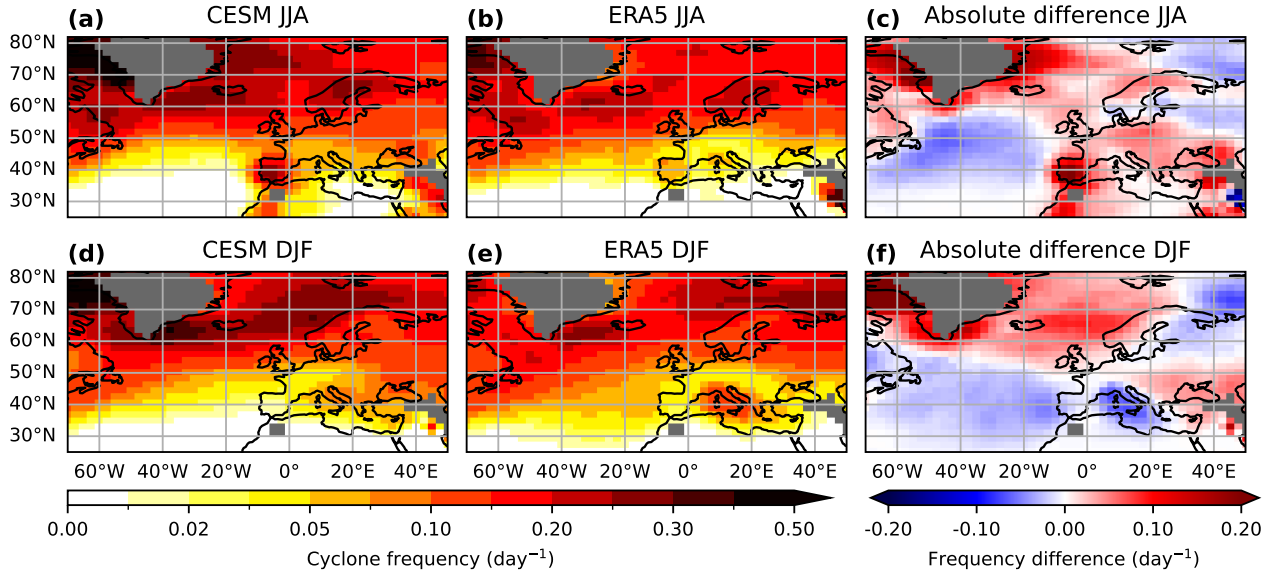
Figure 2. Cyclone frequency [day^{-1}] defined as the number of times a grid cell is located within the calculated radius of a cyclone during the respective season, divided by the number of days of the season in CESM (a,d), ERA5 (b,c) and the difference between CESM and ERA5 (c,f) for summer (JJA; a–c) and winter (DJF; d–f) for the time period 1981–2020. The grey shading indicates areas excluded from the analysis (the model elevation is above 1000 m asl).

On a more regional scale, some noticeable biases are visible. First, CESM strongly overestimates cyclone frequency west of Greenland for all seasons. These signals can mostly be ignored, since most of them are artefacts due to the presence of the Greenland ice sheet. Secondly, in the summer months, the number of cyclones over southern Europe is overestimated, especially over the Iberian Peninsula (Fig. 2c). In the central Mediterranean, the cyclone frequency is underestimated by approximately

225   50% in winter (Fig. 2f). This could be related to the ~~zonal and northward bias of the storm track~~ storm track bias in CESM, and therefore, cyclones from the Atlantic penetrate the Mediterranean too little. The latter would also hamper lee cyclogenesis in the Mediterranean, further explaining the underestimation of cyclone frequency. However, the slight overestimation in the eastern Mediterranean suggests that the ~~zonal~~ storm track bias in CESM only plays a role in the central Mediterranean.

To assess the representation of cyclone characteristics in CESM, we compare several different cyclone-related variables in

230   CESM and ERA5 for the Mediterranean in Fig. 3. CESM slightly overestimates the cyclone lifetime (Fig. 3a–b), while the number of very short-lived cyclones is underestimated in CESM. Maximum cyclone depth is represented well, although it is slightly underestimated in CESM (Fig. 3c–d), apart from JJA where it is generally overestimated. CESM can reproduce the core minimum pressure for DJF (Fig. 3f), showing consistent peaks of maximum and minimum frequencies compared to ERA5. However, larger deviations between CESM and ERA5 are found for JJA, where the peak of the distribution is about 10 hPa

235   higher for CESM compared to ERA5 (Fig. 3e). Larger biases occur for cyclone-related maximum precipitation (Fig. 3g–h) and cyclone-related maximum wind speed (Fig. 3i–j). CESM struggles to reproduce high cyclone-related precipitation events in winter and summer, where the high-end tails of the distributions are most often underestimated by 50%. There is

also an underestimation of cyclone-related high wind speed events in winter and summer, but this bias is less strong than the precipitation bias. Nevertheless, the fact that CESM mostly agrees with ERA5 on cyclone position and strength gives us confidence in the model's representation of cyclones over the Mediterranean.
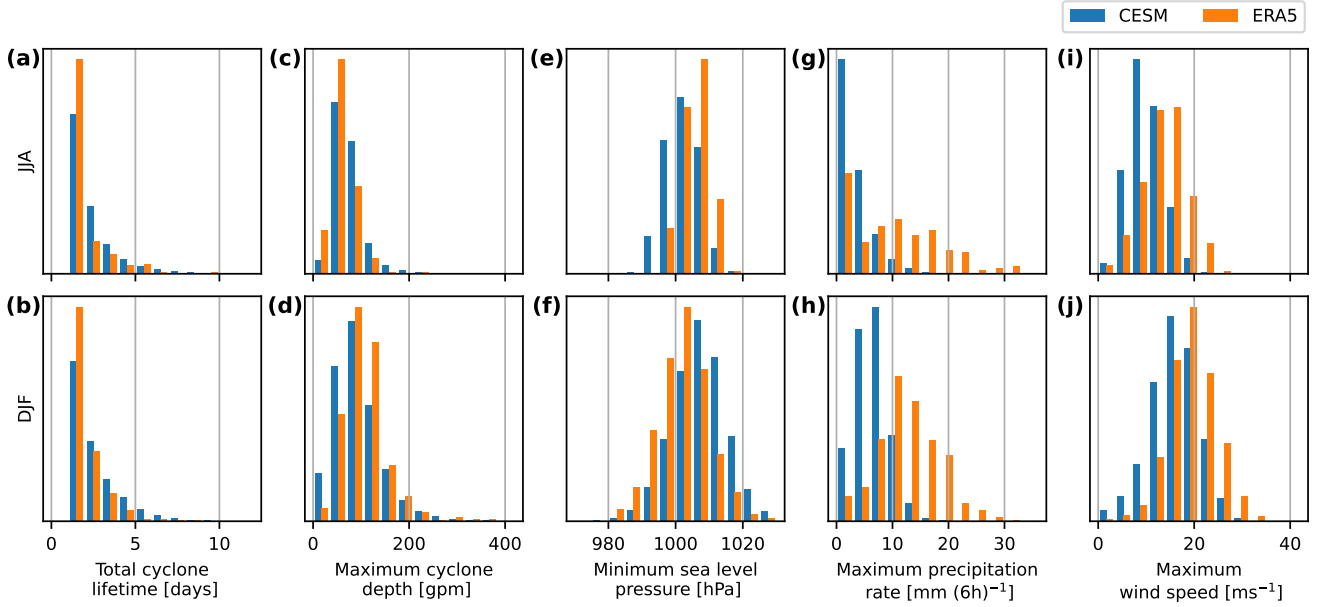
Figure 3. Histograms of Mediterranean cyclone-related features in CESM (blue) and ERA5 (orange) between 1981 and 2010 in JJA (top row) and DJF (bottom row). Shown are the relative frequencies of the total lifetime of the cyclone tracks in days (a–b), maximum cyclone depth during its lifetime in gpm (c–d), minimum sea level pressure during its lifetime in hPa (e–f), Maximum cyclone-related precipitation rate during its lifetime in mm $(6h)^{-1}$ (g–h) and maximum cyclone-related wind speed during at **t0** in ms^{-1} (i–j).

3.2 Internal climate variability in CESM

To show how internal variability and past climate changes affect Mediterranean cyclones, we show 30-year running means of T850 averaged over all grid points of the two boxes (not cyclone related) and several cyclone-related features over the period 1500 BCE to 1850 CE for the two regions combined (Fig. 4). The anomalies are with respect to the averages over the entire 3350-year period. We consider the 30-year running mean of T850 as a proxy for the state of the climate from 1500 BCE to 1850 CE (Fig. 4a). In general, pronounced multi-decadal variability is detected in Fig. 4. Warmer and colder periods alternate, with maximum anomalies in the order of 0.5 °C. The period between 1200 BCE and 500 BCE is dominated by warmer conditions, whereas the period between 1600 CE and 1850 CE is dominated by colder conditions, also known as the Little Ice Age.

The cyclone frequency in the Mediterranean (Fig. 4b) also exhibits clear multidecadal variability. The cyclone frequency in this figure is defined as the total number of grid cells that are occupied by a cyclone centre every month. Cyclone frequency

exhibits a multi-decadal variability that varies in the order of 5%. At the beginning of the simulation, a weak tendency towards a higher number of cyclones is found, whereas, towards the end of the simulation, there is a tendency towards fewer cyclones.
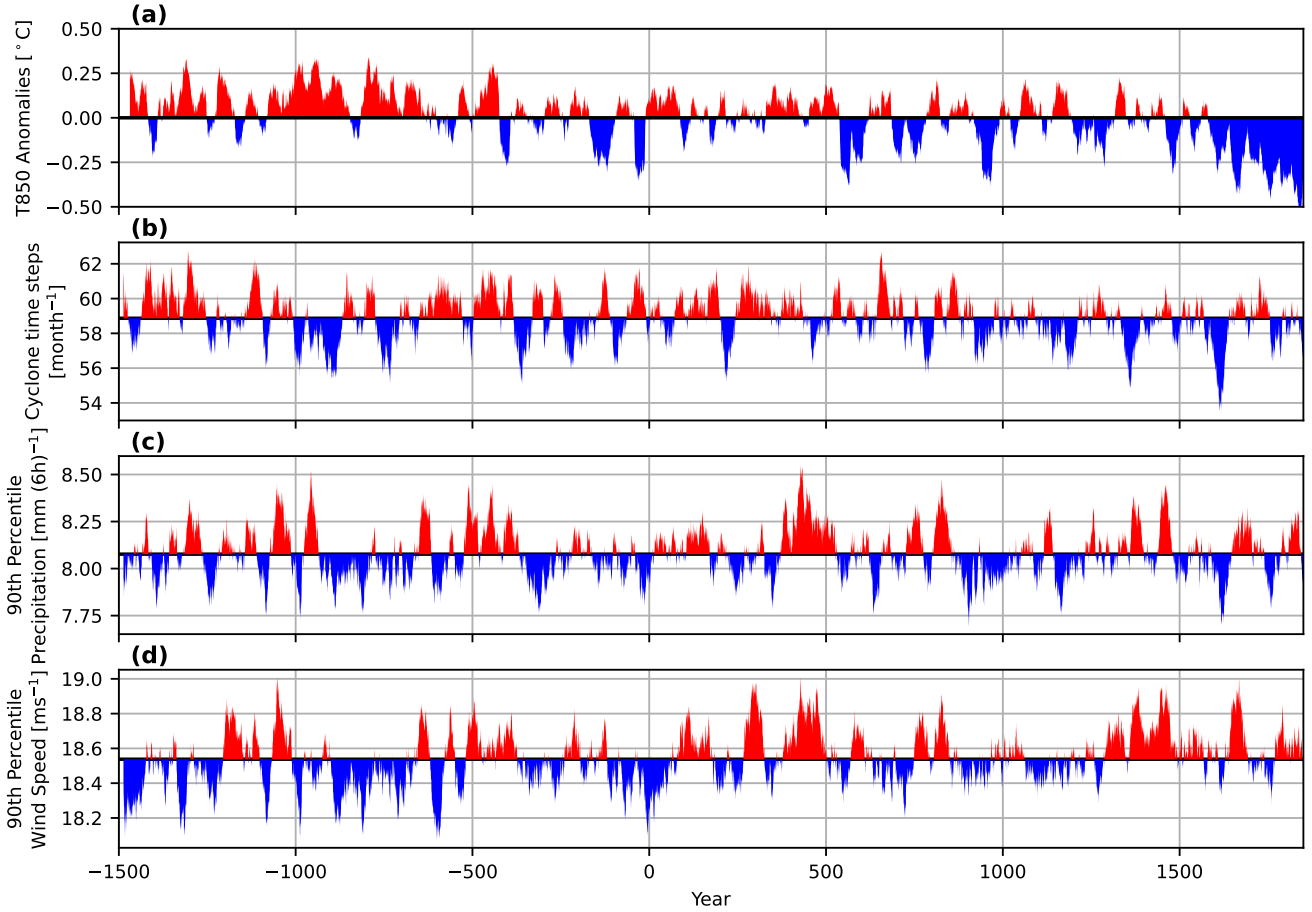
Figure 4. 30-year running means of air temperature and several cyclone-related properties in the central and eastern Mediterranean regions (combined) during 1500 BCE and 1850 CE. Shown are (a) the 850 hPa temperature anomalies in [°C], (b) cyclone frequency in month^{-1}, (c) the 90th percentile of maximum cyclone-related precipitation in mm $(6h)^{-1}$, (d) the 90th percentile of maximum cyclone-related wind speed in m s^{-1}

.

In Fig. 4c and 4d, we present the 30-year running mean of the 90th percentile of monthly maximum cyclone-related pre-
255 cipitation and cyclone-related wind speed, respectively. Identical to the other cyclone-related features, these time series are also dominated by multi-decadal variability. Periods with cyclones that achieve higher precipitation rates and wind speeds often coincide (Table S1). However, these variations are not driven by temperature anomalies or solar irradiance variations (not shown).

3.3 ~~Impact of volcanic eruptions on cyclones~~

~~As volcanic eruptions are known to be an important driver of climate variability, we test whether volcanic eruptions can explain some of the cyclone frequency variability seen in Fig. 4b. We show the mean winter cyclone frequency five years before the 20 strongest eruptions in Fig. ??a, and the mean change in cyclone frequency within two years after these eruptions (Fig. ??b, with hatching showing whether the difference is statistically significant at the 5% level). The mean cyclone frequency of the undisturbed (no volcanic eruptions) years (Fig. ??a) resemble the pattern of the mean winter cyclone frequency in Fig. 2f shows.~~

~~The mean cyclone frequency over northern Europe and the North Atlantic 5 years before the 20 strongest eruptions (a), and the changes in mean cyclone frequency that occur two years after the strongest eruptions (b). The stippling indicates where the changes are statistically significant at the 5% level. All results are for DJF. The grey shading indicates areas excluded from the analysis (the model elevation is above 1000 m asl).~~

~~The changes in cyclone frequency show a clear impact of volcanic eruptions (Fig. ?? b). Over most of Europe, north-eastern North America, and the Arctic Sea, the number of cyclones decreases after a strong volcanic eruption. However, these decreases are only significant in the North Sea and Baltic Sea (at the 5% level). We identify significant cyclone frequency increases over the subtropical Atlantic, the Barents Sea, and the eastern Mediterranean. The significant changes in these regions are in the order of −20 to +50%. Due to the aforementioned biases in Fig. 2 around the Greenland ice sheet, we ignore the large frequency increase west of Greenland. Only a small region with a significant increase in cyclone frequency is found in the eastern Mediterranean, but it still accounts for an increase of 30% in this region.~~

3.3 Atmospheric modes of circulation and cyclone features

Since the large-scale variability can be another important influence on Mediterranean cyclone frequency, we show the statistical relationships of the four most dominant modes of circulation in the North Atlantic European region with extratropical cyclones for DJF (Fig. 5). The modes are calculated with an EOF-analysis applied to the CESM Z500 fields (see section 2). The patterns resemble the North Atlantic Oscillation (NAO), East Atlantic pattern (EA), East Atlantic Western Russia pattern (EAWR), and the Scandinavian pattern (SCAN) (Fig. S1). The NAO explains most of the variability in Z500 in DJF with 26.8 % (Fig. 5a), which is in agreement with previous studies (i.e. Barnston and Livezey (1987)). The NAO is followed by the SCAN-pattern (11.8 %, Fig. 5d), the EA-pattern (10.8 %, Fig. 5b), and the EAWR-pattern (9.6 %, Fig. 5c).

Correlation Atmospheric Modes and Cyclone Frequency DJF
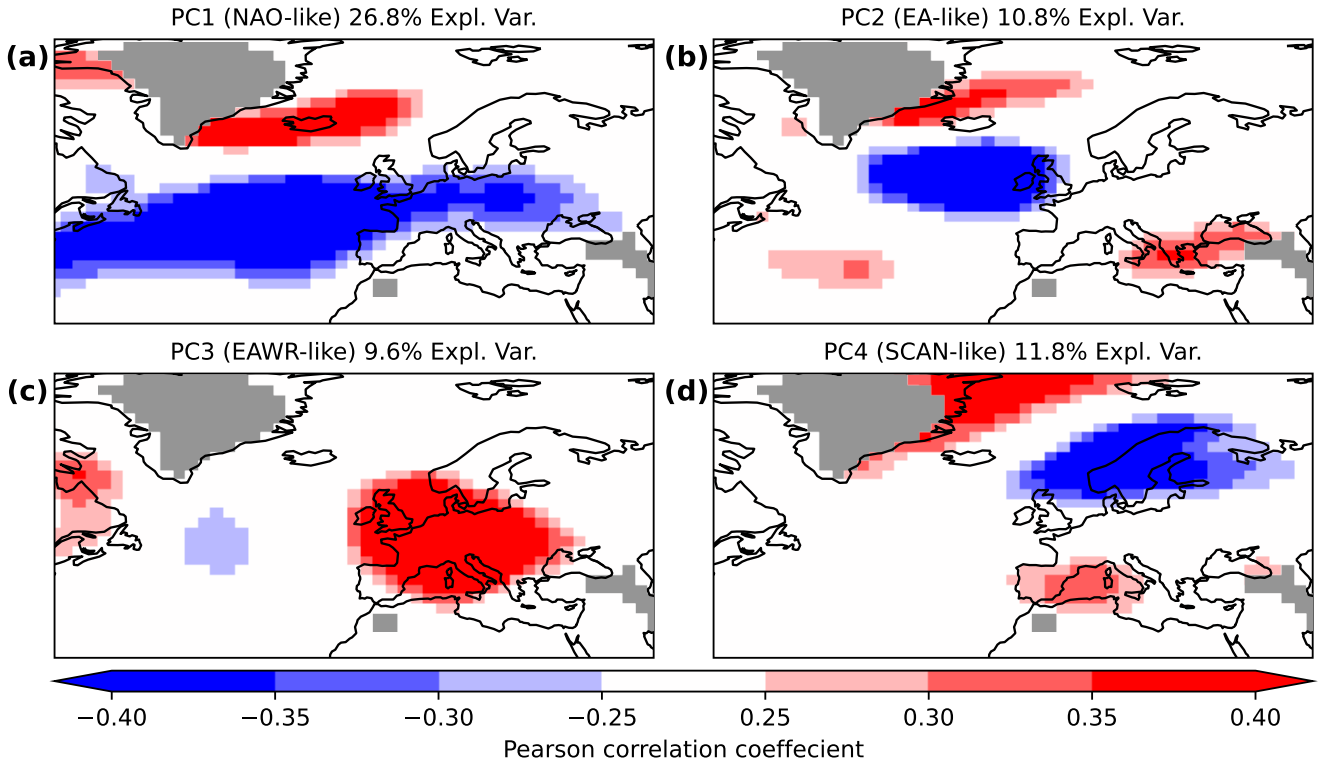
Figure 5. The principal components that represent the (a) North Atlantic Oscillation (NAO), (b) East Atlantic pattern (EA), (c) East Atlantic Western Russia pattern (EAWR), and (d) Scandinavian pattern (SCAN) correlated to the local cyclone frequency in day^{-1} using the Pearson correlation analysis. Red shading indicates a positive correlation, whereas blue colours indicate a negative correlation. The grey colours indicate grid cells with model topography above 1000 m (excluded from the analysis). All results are for DJF. The mean structures of the different patterns are shown in Supplementary Figure S1.

The NAO shows the highest correlation with cyclone frequency over the North Atlantic and central Europe (Fig. 5a). A strong negative correlation is found between the NAO and cyclone frequency over the Atlantic between 30° N and 50° N (Fig. 5a), implying a northward shift of the jet when the NAO is in a positive state, and vice versa. The EA mode is less impactful than the NAO on cyclone frequency (Fig. 5b). A positive EA phase is related to a decrease in cyclone frequency over the North Atlantic, whereas the area north of Iceland exhibits an increase in cyclone frequency. There is also an indication that cyclone frequency increases in the subtropical Atlantic and the eastern Mediterranean during a positive EA phase and vice versa during a negative phase. The EAWR mode (Fig. 5c) exhibits a strong positive correlation with cyclone frequency over central Europe and the central Mediterranean, where a positive EAWR phase leads to an increase of cyclones in this area. Lastly, the SCAN mode is negatively correlated with cyclone frequency over Scandinavia, and positively correlated with cyclone frequency in

the Arctic Sea and the western Mediterranean (Fig. 5d). We found no significant correlation between the 4 modes in Fig. 5 and cyclone-related precipitation or wind speed in the Mediterranean, and therefore they are not shown.

For JJA, we find very similar patterns to those during DJF for the correlation between the atmospheric modes and cyclone frequency (Fig. S2). The main differences to DJF are that the atmospheric modes explain less variance due to the more chaotic nature of the atmosphere in summer and, therefore, the correlations are less strong. We do not find any significant correlations for the Mediterranean in JJA.

4   Extreme Mediterranean cyclones

In the previous sections, we mainly focused on the impact of climate variability on Mediterranean cyclones. Here, we shift the focus to the most extreme cyclones that can occur under climate conditions of the late Holocene. In Fig. 6a–f, we show wind speed and precipitation composites for the EXC100 for the period 1500 BCE–1850 CE during DJF. Although these composites correspond to three distinct EXC types (precipitation, wind speed and compounding events), it is important to acknowledge that an individual EXC may appear within the top 100 rankings across multiple metrics (Table S2).

In the composites, we see the general characteristics of an extratropical cyclone. The highest wind speeds are found on the southeastern flank of the EXC100. On the contrary, lower wind speeds are found on the northern flank of the EXC100 (Fig. 6a–f). The most intense precipitation is present just east of the cyclone core (Fig. 6g–l). However, typical structures associated with extratropical cyclones, such as fronts, are hard to identify due to the low horizontal resolution of the model. When comparing the composites between the regions, some notable differences are found. Generally, EXC100s in the central Mediterranean are stronger in terms of wind speed than EXC100s in the eastern Mediterranean. Wind speed EXC100s (Fig. 6b) in the central Mediterranean exceed 25 ms^{-1}, whereas they barely exceed 20 ms^{-1} in the eastern Mediterranean (Fig. 6e). EXC100s are statistically significantly stronger in the central Mediterranean for the southeastern flank of the cyclone. However, wind speed EXC100s in the eastern Mediterranean are significantly stronger on the northern flank (Fig. 6e).
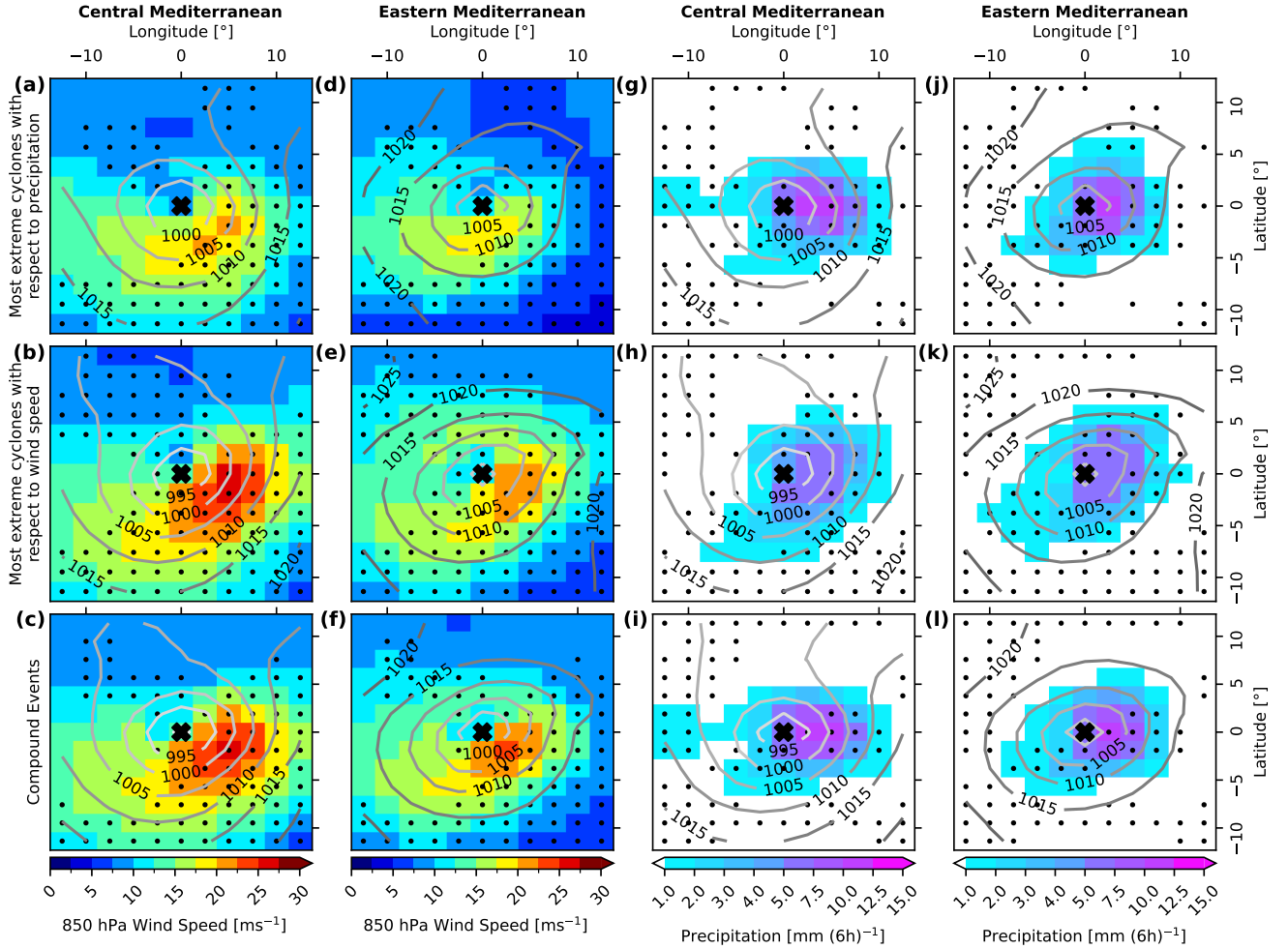
Figure 6. Composite analysis for the 100 most extreme cyclones (EXC100) for the period 1500 BCE–1850 CE in the central Mediterranean (a–c and g–i), and the eastern Mediterranean (d–f and j–l). For wind speed extremes we use the time when the cyclone achieves minimal sea level pressure (**t0**); for precipitation extremes we use the time step where maximum precipitation occurred. For composite events, we show the wind speed at **t0**), and the precipitation the time step where maximum precipitation occurred. The EXC100 are estimated with respect to precipitation (top row), wind speed (middle row), and compounding events (bottom row). In panels a–f, the colour shading shows WS850, and in panels g–l, the colour shading indicates 6-hourly precipitation. The stippling indicates where the difference for one event type is statistically significant at the 5% level between the two regions. The grey contours indicate the composite mean sea level pressure.

315 It must be noted that the region defined as the central Mediterranean in Fig. ~~??b~~ 1 is located more north and, therefore, may be more heavily influenced by the stronger midlatitude storm tracks. Secondly, wind speed and compounding EXC100s tend to have a lower core pressure than precipitation EXC100s in the order of 5 hPa. This holds true for both the EXC100s in the

central and eastern Mediterranean. Compounding EXC100s show a similar pattern compared to wind speed EXCs for both regions.

320 As expected, precipitation EXC100s have much higher precipitation rates than wind speed EXCs with differences of up to 10 mm (6h)$^{-1}$. Compounding EXCs tend to produce precipitation rates comparable to those of EXCs with respect to precipitation. Differences between the central and eastern Mediterranean are statistically significant (5% level) for precipitation EXCs, but compared to wind speed EXCs, the grid cells that are significantly different are more randomly dispersed (stippling in Fig. 6).

325 The EXC100 composites for JJA show much lower extreme values with respect to wind speed and precipitation (Fig. S3). The differences for wind speed and precipitation are in the order of 50% or more. This is expected since cyclones in the Mediterranean are less extreme in summer compared to winter. However, EXC100s in the central Mediterranean produce stronger wind speeds and precipitation rates than in the eastern Mediterranean, where the cyclone barely appears in the composites in either sea level pressure, precipitation or wind speed.

330 To characterize the life cycle of extreme cyclones, we show the temporal evolution of EXC10, EXC100, and EXC1000 in the central and eastern Mediterranean during DJF (Fig. 7). We do this by selecting the most extreme value from each composite for every time step. Precipitation peaks about 6 hours before **t0** (Fig. 7a–c), whereas wind speed peaks at **t0** (Fig. 7d–f). Interestingly, for wind speed EXCs, precipitation in the central Mediterranean tends to peak 12 hours earlier than in the eastern Mediterranean (Fig. 7b). For precipitation, hardly any significant differences between the central and eastern

335 Mediterranean can be found for the EXC100 for either precipitation, wind speed, or compounding events (Fig. 7a–c). However, the differences between the EXC1000 are significant most of the time with EXC1000s producing more precipitation in the central Mediterranean, indicating a structural difference between less extreme cyclones in the two regions. In Fig. 7c, EXC10 stands out in terms of extremeness in precipitation in the central Mediterranean, as it reaches a maximum of around 15 mm (6h)$^{-1}$, although EXC10 shows little statistical significance along its track between the central and eastern Mediterranean for

340 both precipitation and wind speed (Fig. 7a–f). Another notable difference between the eastern and central Mediterranean is that precipitation before **t0** is generally higher in the central Mediterranean compared to the eastern Mediterranean (especially for wind speed and compounding EXC100s and EXC1000s in Fig. 7b and c), with differences of a few mm (6h)$^{-1}$. However, the difference after **t0** dissipates.
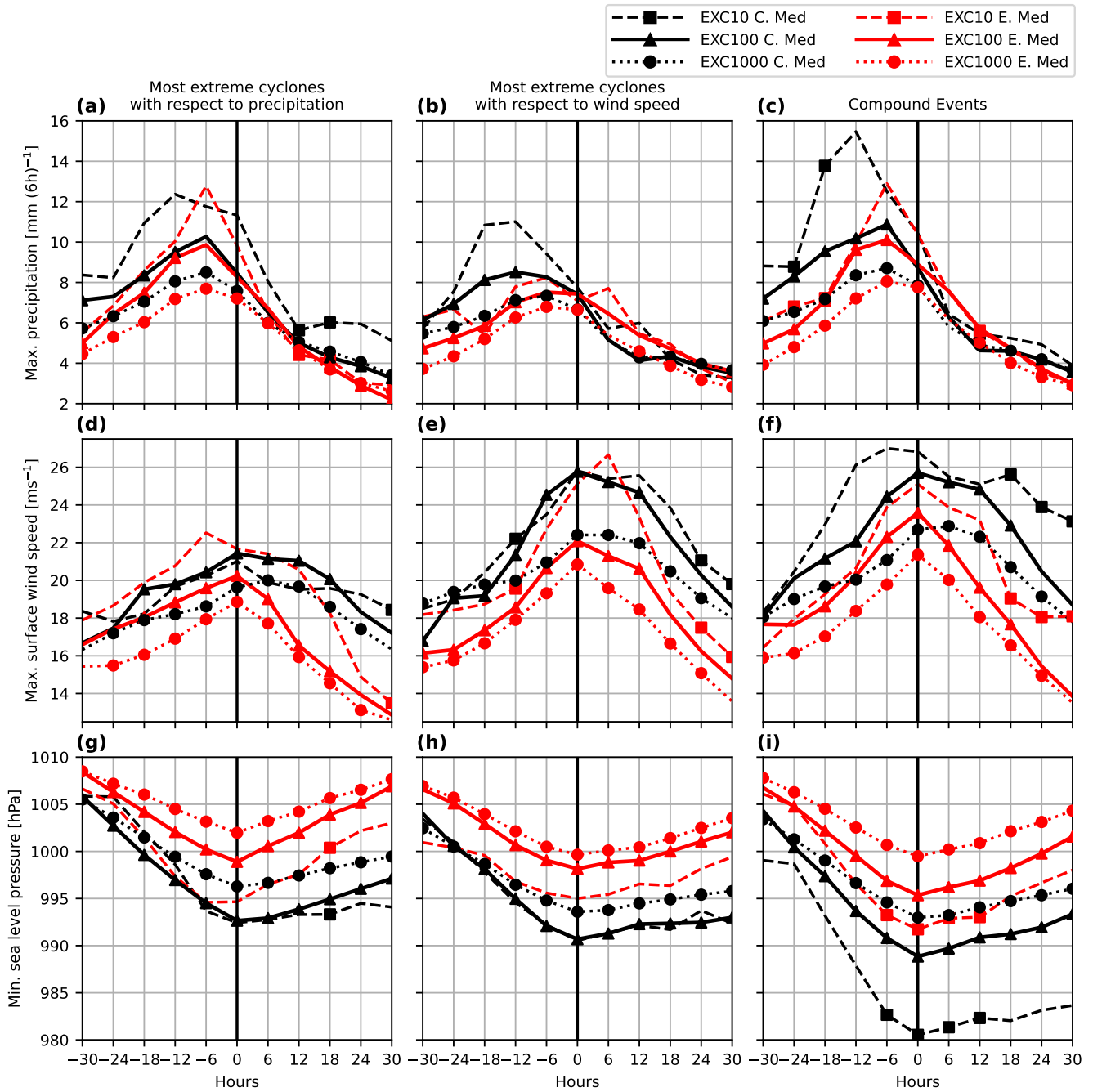
Figure 7. The evolution of three extreme cyclone statistics in the central Mediterranean (in black) and the eastern Mediterranean (in red). The values indicate the most extreme value of every composite for 6-hourly precipitation in mm $(6h)^{-1}$ (a–c), 850 hPa wind speed in ms^{-1} (d–f), and sea level pressure in hPa (g–i) for precipitation EXCs (left column), wind speed EXCs (middle column) and compounding EXCs (right column). The results are shown from 30 hours before the extreme cyclone's minimum SLP until 30 hours after the extreme cyclone's minimum SLP. The values for EXC10 (dashed line), EXC100 (solid line) and EXC1000 (dotted line) are shown. The markers indicate whether the difference between EXC10 (square), EXC100 (circle), and EXC1000 (triangle), respectively, are statistically significant at the 5% level between the regions for a point in time.

When looking at wind speed (Fig. 7d–f), the higher wind speeds in the central Mediterranean from Fig. 6 appear throughout
the entire cyclone life span for all precipitation, wind speed and compounding EXCs. These differences are significant for
EXC100 and EXC1000 for most of their life cycle. Contrary to precipitation in Fig. 7a–c, these differences are also evident
after t0 and become even larger.

EXCs deepen quickly in terms of SLP before t0, whereas they fill up more slowly after t0 (Fig. 7g–i). SLP is generally
lower in the central Mediterranean than in the eastern Mediterranean, which may be due to the more southern location of the
eastern Mediterranean region defined in Fig. ~~2~~1. Interestingly enough, differences between EXC10, EXC100, and EXC1000
are larger for compounding events than precipitation or wind speed EXCs, especially in the central Mediterranean.

Considering the temporal evolution during summer (Fig. S4), the differences between the eastern Mediterranean and the
central Mediterranean are small for precipitation EXC100s, although they consistently produce more precipitation in the central Mediterranean during their lifetime (Fig. S4a). In contrast to DJF (Fig. 7a,c), precipitation also peaks at t0 for precipitation
and compounding EXCs. The differences between the two regions for wind speed EXCs and compounding events are large.
EXC10s and EXC100s produce much higher wind speeds for wind speed EXCs and, to a lesser extent, compounding events
in the central Mediterranean compared to the eastern Mediterranean (Fig. S4e–f). Still, apart from wind speed EXC10s and
EXC100s in the central Mediterranean (Fig. S4e), wind speed and precipitation are in the order of 50% less over the whole
cyclone lifetime in JJA compared to DJF (Fig. 6). Interestingly, neither in the central Mediterranean nor in the eastern Mediterranean do SLPs fall during the deepening phase, and neither do they rise again after t0 (Fig. S4g–i). Wind and compounding
EXCs in JJA seem to be only able to produce wind speeds higher than 15 ms^{-1} in the central Mediterranean. It must be noted
that our model is far too coarse to properly capture convective processes, which play an important role in summer, possibly
leading to a misrepresentation of cyclone-related precipitation in JJA.

To identify what drives the differences between the regions and the EXC types, we show the EXC100 composites of the
conditions in the upper atmosphere. In Fig. 8a–f, cold air masses are located northwest of the EXC100 centre and warm air
masses are located southeast of the EXC100 centre, highlighting the warm and cold sectors of the cyclones. The highest WS300
values are found south of the EXC100 centre, indicating that the jet stream is usually located south of the EXC100 centre.

The differences between the central and eastern Mediterranean in Fig. 8a–f are large. The jet stream south of the EXC100
centre in the eastern Mediterranean (up to 50 ms^{-1}) is much stronger than over the central Mediterranean (up to 40 ms^{-1}).
Also, the jet stream is located southeast of the EXC100 centre in the eastern Mediterranean, whereas the jet stream in the
central Mediterranean is only located south and southwest of the EXC100 centre. Given the location of our areas of interest,
EXC100s in the eastern Mediterranean are generally located more south and closer to the subtropical jet. This explains the
higher WS300 values in the eastern Mediterranean. Another difference between the two regions is that EXC100s in the eastern
Mediterranean are related to much stronger intrusions of cold air in the lower troposphere northwest of the EXC100 centre
(more than -8 °C compared to -4 °C in the central Mediterranean). Although the negative T850 anomalies are stronger over the
eastern Mediterranean, EXC100s over the central Mediterranean are accompanied by stronger positive T850 anomalies over
the southeastern flank of the EXC100 centre (more than 4 °C compared to 2 °C in the eastern Mediterranean).

100 most extreme cyclones in the Mediterranean
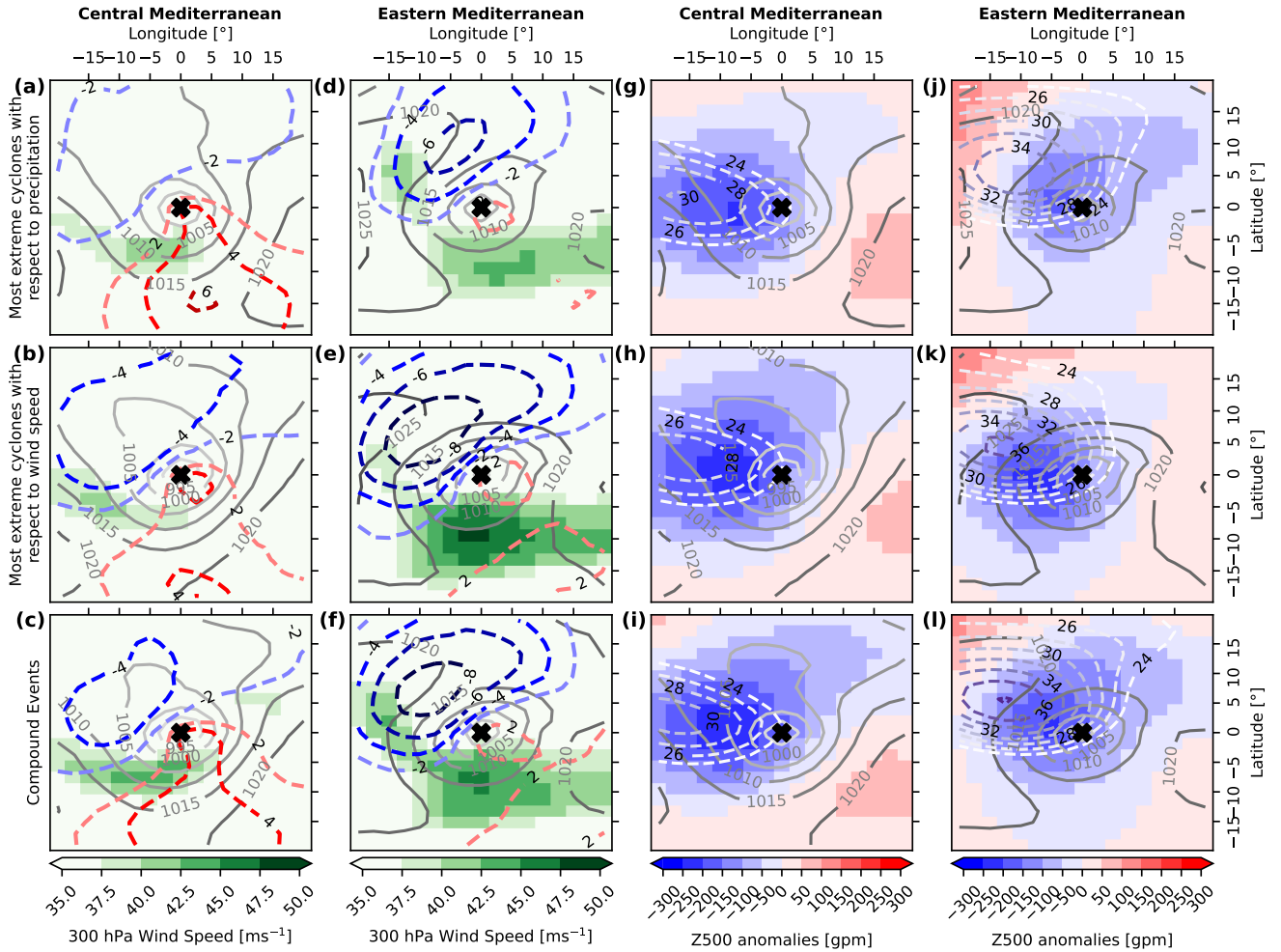
Figure 8. Same as Fig. 6 but now for 300 hPa wind speed in ms⁻¹ (green shading), and 850 hPa temperature anomalies in °C (red and blue contour lines) in panels a–f. In panels g–l, red-blue shadings show the 500 hPa geopotential height anomalies in gpm and the dashed white contour lines show the Rossby wave packet amplitude in ms⁻¹. The grey contour lines indicate the SLP in all panels.

In Fig. 8g–l, the cyclone centres are often located just east of the lowest Z500 anomalies and the maximum RWP amplitude, highlighting a westward tilting of the cyclone in the upper atmosphere that indicates that these cyclones grow baroclinically.

380 Also, EXC100 composites are accompanied by weak positive Z500 anomalies southeast of the EXC100 centre.

Wind speed EXC100s are associated with higher WS300 values and T850 gradients. This indicates that precipitation EXC100s require less dynamical forcing than wind speed EXC100s. Interestingly, positive T850 anomalies within the warm sector do not differ between EXC100 subtypes within the regions, whereas negative T850 anomalies within the cold sector are usually stronger for wind speed EXC100s and compounding EXC100s than for precipitation EXC100s.

EXC100s in the central Mediterranean are accompanied by a spatially larger negative Z500 anomaly than in the eastern Mediterranean. Precipitation EXC100s are associated with less strong Z500 anomalies than the other two EXC100 types (only going up to 200 gpm). The Z500 anomalies for precipitation EXCs in the eastern Mediterranean are especially small in size.

Negative Z500 anomalies are often associated with troughs, which can be linked to intruding Rossby waves, explaining why an RWP is present for all EXC100 types and regions. The centre of the RWP is located slightly west of the centre of the Z500 anomaly. RWPs for EXC100s in the eastern Mediterranean have a larger amplitude (up to 38 ms^{-1}) than EXC100s in the central Mediterranean (up to 30 ms^{-1}). This indicates that intruding Rossby waves play a crucial role in cyclone development in the eastern Mediterranean. Strikingly, the RWP amplitude between EXC100 types for the same regions seems to be similar. It seems that compounding EXCs in the eastern Mediterranean (Fig. 8l) are associated with a slightly stronger RWP amplitude than precipitation and wind speed EXCs (Fig. 8j–k). However, this difference is small and cannot be seen in the central Mediterranean.

The EXC100 composites for the upper-atmosphere during JJA (Fig. S5) show generally lower values for WS300, T850 anomalies, Z500 anomalies, and RWP amplitude compared to the EXC100 composites in Fig. 8. The only exceptions here are the T850 anomalies for the central Mediterranean that are stronger in JJA by about 2 °C (Fig. S5a–c). Also, the relative differences between JJA and DJF are much larger in the eastern Mediterranean compared to the central Mediterranean. The difference between the two seasons indicates that the upper-atmosphere related to EXCs is much less dynamically active in summer, leading to fewer extreme cyclones. However, in JJA, the WS300 and the RWP amplitude composites are strongest in the central Mediterranean, in contrast to DJF where WS300 and RWP amplitude are strongest in the eastern Mediterranean, suggesting the subtropical jet plays a much smaller role in the eastern Mediterranean in summer. The jet stream only plays a role for EXC100s with respect to wind speed in the eastern Mediterranean (Fig. S5e).

In Fig. 9, we show the time series of the maxima in WS300 (Fig. 9a–c) and RWP amplitude (Fig. 9d–e) during the cyclone lifetime. As already shown in Fig. 8, we find that at $t0$, the values for RWP amplitude and WS300 are higher in the eastern Mediterranean than in the central Mediterranean. Generally speaking, this holds true for most of the EXC life cycle. However, there are some exceptions to this. For the EXC100, the differences are only statistically significant for the wind speed EXCs (Fig. 9b). Also, after $t0$, WS300 increases for all EXC event types in the eastern Mediterranean, leading to a larger difference for WS300 between the eastern and central Mediterranean. Also, there is only a small difference between WS300 values for EXC10, EXC100, or EXC1000 during the life cycle of a cyclone in the eastern Mediterranean (compound events being the only exception). In the central Mediterranean, only the EXC10 stand out in terms of WS300 values. This would imply that the strength of the jet stream only plays an important role for the most extreme cyclones.
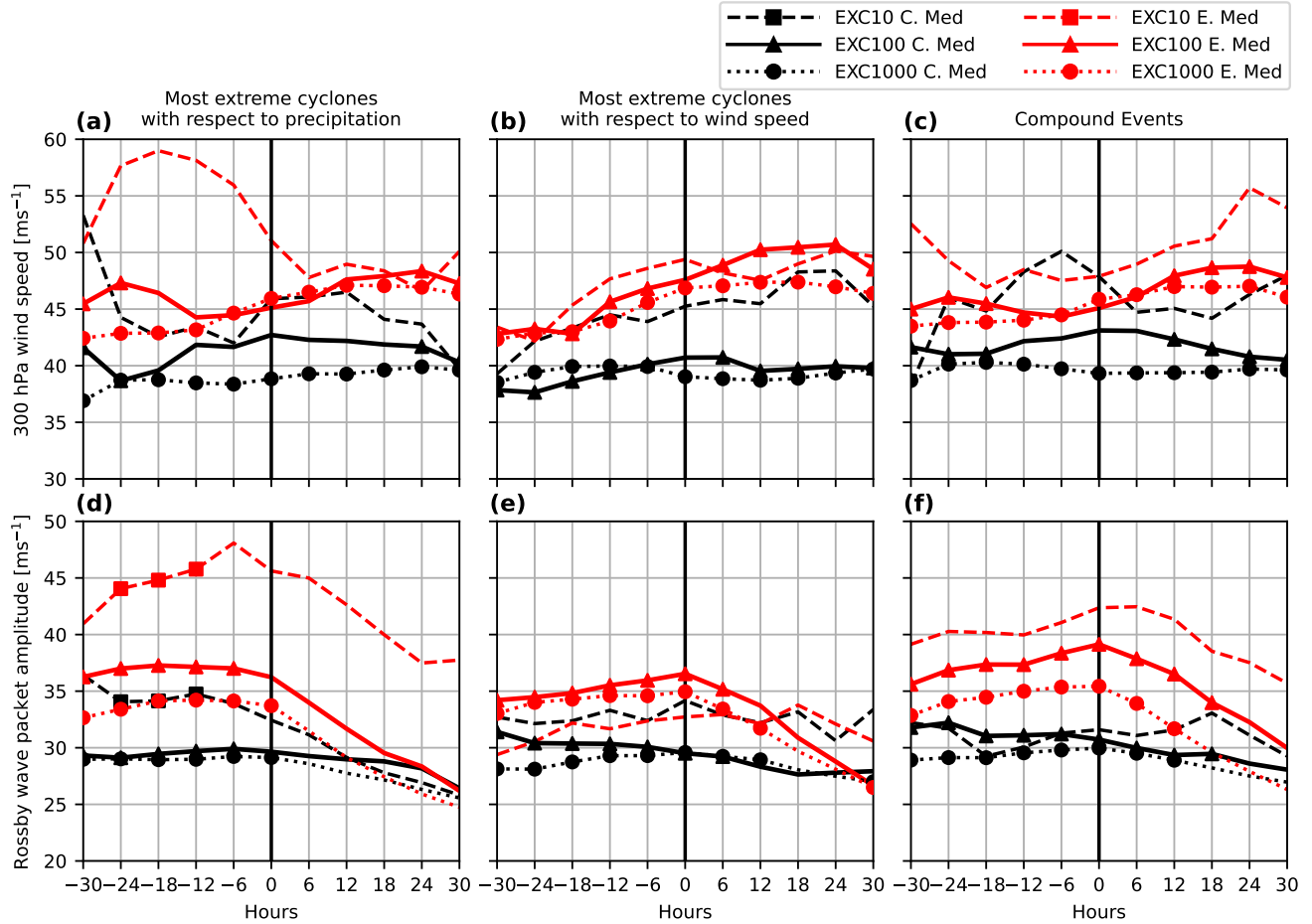
Figure 9. Same as Fig. 7 but now for 300 hPa wind speed in ms^{-1} (a–c), and Rossby wave packet amplitude ms^{-1} (d–f).

Throughout the entire EXC life cycle, the RWP amplitude is also higher in the eastern Mediterranean compared to the central Mediterranean. This difference is significant for wind speed and compounding EXC100s. After $t0$, this gap diminishes, indicating that the peak RWP amplitude plays a stronger role in EXC development for the eastern Mediterranean than for the central Mediterranean.

The temporal evolution of WS300 and RWP amplitude during JJA is similar to the temporal evolution in Fig. 9. WS300 values stay more or less constant during the whole cyclone lifetime, whereas maximum RWP amplitude decreases after $t0$. One exception, is the RWP amplitude in the eastern Mediterranean, that stays around 15 ms^{-1}. The main differences compared to DJF are that maximum values for WS300 and RWP amplitude are lower and that the regions with the highest values are the central Mediterranean compared to the eastern Mediterranean in DJF.

5 Discussion and conclusion

In this study, the impact of climate variability on Mediterranean cyclones is analysed for the period from 1500 BCE to 1850 CE using CESM. Moreover, we present the major characteristics of extreme cyclones in the region for this time period. While substantial research has explored how present and future climatic states affect the occurrence and intensity of Mediterranean cyclones (Raible et al., 2010; Lionello et al., 2016; Hochman et al., 2020), this study is novel in providing a baseline for Mediterranean cyclones within a multi-millennium perspective not affected by anthropogenic global warming.

We find that periods with higher and lower cyclone frequency and intensity in the Mediterranean exhibit a clear multi-decadal variability in the order of 5% from the multi-millennial mean. The dominant atmospheric modes of atmospheric circulation in the Atlantic European region only explain some of the variance in cyclone frequency in the Mediterranean, whereas they show stronger correlations with cyclone frequency in the North Atlantic and northern Europe. ~~Volcanic eruptions can cause a significant increase in cyclone frequency in the eastern Mediterranean, but for the Mediterranean as a whole, the signal is rather weak. Generally, we find significant impacts of volcanic eruptions over large parts of North America, the Atlantic Ocean, and its neighbouring seas.~~

Raible et al. (2018) used an older version of CESM but with a higher horizontal resolution ($1.0° \times 1.0°$) to track cyclones in the North Atlantic and over Europe. The biases they observed are similar to the results presented here, with an overestimation of cyclone frequency near the Greenland ice sheet and ~~CESM being too zonal and the jet being shifted too far northward . We have shown that compared to~~ a northward shift of the storm tracks. Compared to the ~~our model simulation and the~~ ERA5 reanalysis we have show that our cyclone detection and tracking algorithm within our model simulation captures the extreme cyclones in the Mediterranean ~~Sea~~ region well, even though the horizontal resolution of the climate model used is too coarse, as discussed in Flaounas et al. (2013). However, it should be noted that the cyclone-related precipitation and wind speed in CESM are underestimated compared to ERA5. The weak relations between the cyclone frequency and the most dominant modes of circulation in the Mediterranean are similar to those found by Seierstad et al. (2007) and Walz et al. (2018). However, the low resolution of our model may hamper the ability to find further relations between cyclone frequency and modes of circulation. ~~Additionally, it should be noted that the cyclone-related precipitation and wind speed in CESM are underestimated compared to ERA5. It is reported that in CMIP5 models with relatively coarse horizontal resolutions, the winter North Atlantic storm tracks tend to show a too zonal structure or a southward displacement (Zappa et al., 2014; Müller et al., 2018). These biases also influence the NAO variability, which is related to the extratropical and Mediterranean cyclone variability. Although the CESM version with its coarse resolution used in our study shows the same issue, it still provides a long transient simulation of the last 3350 years, therefore, allowing investigating long-term temporal variability of cyclones and related features.~~

We also find that the variability of Mediterranean cyclones is very similar to what Raible et al. (2018) observed for North Atlantic cyclones in the aforementioned earlier version of CESM. They revealed that the cyclone variability is not driven by solar irradiance variations. Our results show no significant relationship between the Mediterranean cyclone variability and solar irradiance, which confirms the aforementioned study. ~~Raible et al. (2018) found no imprint of volcanic eruptions on cyclone frequency contradicting our results. Andreasen et al. (2024) found an increase in cyclones over the subtropics and high latitudes~~

~~and a decrease over the mid-latitudes after volcanic eruptions due to larger meridional temperature gradients and a lower tropopause. This is much more in line with our results. Though it must be noted that the eruptions in Andreasen et al. (2024) are much stronger than the eruptions in the simulation of Raible et al. (2018) who consider eruptions after 850 CE. This also could~~ [460] ~~explain why our result is more similar to Andreasen et al. (2024), as our simulation includes stronger eruptions due to the longer time span~~ It is reported that in CMIP5 models with relatively coarse horizontal resolutions, the winter North Atlantic storm tracks tend to show a southward displacement and too few cyclones in the Mediterranean (Zappa et al., 2014; Müller et al., 2018). Despite our model showing a northward bias, it also produces too few cyclones in the Mediterranean. These biases influence the NAO variability, which is related to the extratropical and Mediterranean cyclone variability. Still our simulation provides a [465] long transient simulation of the last 3350 years, therefore, allowing investigation of long-term temporal variability of cyclones and related features.

Our extreme cyclone (EXC) composites show that wind speed EXCs are generally stronger in the central Mediterranean compared to the eastern Mediterranean. The difference between the two regions for precipitation EXCs is much less clear, and overall, there does not seem to be a large difference between the two regions for precipitation EXCs. On average, precipitation [470] tends to peak 6 to 12 hours earlier than $t0$. This is consistent with Messmer and Simmonds (2021) and Raveh-Rubin and Wernli (2015), who found that precipitation peaks before wind speed in the ERA5 reanalysis, and with Booth et al. (2018), who showed that the precipitation on average peaks 12 hours prior to the dynamical strength maximum of a cyclone based on satellite data. Our findings indicate that EXCs in the central Mediterranean can have a higher potential impact on society, mainly due to their higher potential wind speeds. This is amplified by the fact that EXCs in the central Mediterranean tend to [475] be more extreme in terms of wind speed over their entire life cycle and not only at $t0$.

Flaounas et al. (2015b) performed a similar composite analysis of intense cyclones using a regional model with a higher horizontal resolution (20 km horizontal resolution) but considering the Mediterranean basin as a whole for the period ~~1898–2008~~ 1989–2008. Despite the higher resolution, the structure and the location of the area with the most intense precipitation are similar to the results presented here, which gives us confidence in the ability of CESM to produce extreme cyclones despite the low reso- [480] lution of our model. They also suggest that the subtropical jet might play a crucial role in cyclone development by providing barotropic shear. Despite the fact that the subtropical jet is clearly more dominant in the eastern Mediterranean in winter, this does not result in stronger cyclones over the region and may not be the driving factor for the development of EXCs.

Homar et al. (2007) showed that the central Mediterranean experiences more intense Mediterranean cyclones than the eastern Mediterranean. This is in line with our results where we observe more intense wind speed EXCs in the central Mediterranean, [485] since wind speed EXCs require a deeper and better developed cyclone than precipitation EXCs. However, Flaounas et al. (2023) showed that there is no difference between the two regions in the occurrence of intense cyclones using composite tracks in the ERA5-reanalysis. Nevertheless, our simulation has the advantage that, due to the long time period, the effect of natural variability should be averaged out, adding to the hypothesis of Homar et al. (2007).

To conclude, there is no obvious single driver of Mediterranean cyclone variability. Mediterranean cyclones vary on multi- [490] decadal timescales around roughly 5% from the multi-millennial mean. Additionally, our findings indicate that cyclones may have a stronger socio-economic impact in the central Mediterranean than in the eastern Mediterranean, especially in terms of

wind speed extremes. Our study offers a climatological reference baseline for understanding extreme cyclones in the region. Having this reference baseline is also beneficial for quantifying the effects of future climate change on Mediterranean cyclones. Nonetheless, the low resolution of the model simulation used is a major drawback. Thus, future work on the long-term variability of cyclones using a higher-resolution model is needed, as pointed out by Flaounas et al. (2013). For instance, a regional climate model can be used to downscale parts of this CESM simulation to provide more realistic insights into extreme Mediterranean cyclones and their intensification processes.

Code availability. The cyclone tracking was performed with the detection and tracking scheme of Blender et al. (1997) and is available on request. The other analysis steps were performed with python scripts. As they are standard methods, they are not uploaded to a repository. These scripts are available on request.

Data availability. The ERA5 data are provided by Copernicus Climate Change Service Climate Data Store (CDS) from their website at https://cds.climate.copernicus.eu (last access: 9 Nov 2023). Post-processed CESM and ERA5 data used for the study are available at https://doi.org/10.5281/zenodo.13619444 Complete CESM1.2.2 data are locally stored and are available upon request

Author contributions. OD, MM, WMK, and CCR contributed to the design of the study. WMK carried out the climate simulations. OD performed the principal analysis and wrote the manuscript under the supervision of CCR. MM, WMK, and CCR provided critical feedback on the results and drafted the manuscript together with OD. All authors contributed to the writing and scientific discussion.

Competing interests. The authors declare no conflict of interest.

Acknowledgements. We acknowledge the Swiss National Supercomputing Centre (CSCS) in Lugano, Switzerland, for providing the necessary computational resources and supercomputing architecture to perform the simulations under project number s1248. OD and CCR received funding from the Swiss National Science Foundation (grant nos. 200020_172745 and IZCOZ0_205416).

References

2k PMIP3 group, P.: Continental-scale temperature variability in PMIP3 simulations and PAGES 2k regional temperature reconstructions over the past millennium, Climate of the Past, 11, 1673–1699, https://doi.org/10.5194/cp-11-1673-2015, 2015.

Alpert, P. and Ziv, B.: The Sharav cyclone: observations and some theoretical considerations, Journal of Geophysical Research: Atmospheres, 94, 18 495–18 514, https://doi.org/10.1029/JD094iD15p18495, 1989.

Andreasen, L. S., Cornér, J., Abbott, P., Sinclair, V. A., Riede, F., and Timmreck, C.: Changes in Northern Hemisphere extra-tropicalcyclone frequency following volcanic eruptions, Environmental Research: Climate, 3, https://doi.org/10.1088/2752-5295/ad2c0e, 2024.

Barnston, A. G. and Livezey, R. E.: Classification, seasonality and persistence of low-frequency atmospheric circulation patterns, Monthly weather review, 115, 1083–1126, https://doi.org/10.1175/1520-0493(1987)115<1083:CSAPOL>2.0.CO;2, 1987.

Blender, R., Fraedrich, K., and Lunkeit, F.: Identification of cyclone-track regimes in the North Atlantic, Quarterly Journal of the Royal Meteorological Society, 123, 727–741, https://doi.org/10.1002/qj.49712353910, 1997.

Booth, J. F., Naud, C. M., and Jeyaratnam, J.: Extratropical cyclone precipitation life cycles: A satellite-based analysis, Geophysical Research Letters, 45, 8647–8654, https://doi.org/10.1029/2018GL078977, 2018.

Brandimarte, L., Di Baldassarre, G., Bruni, G., D'Odorico, P., and Montanari, A.: Relation between the North-Atlantic Oscillation and hydroclimatic conditions in Mediterranean areas, Water Resources Management, 25, 1269–1279, https://doi.org/10.1007/s11269-010-9742-5, 2011.

Campins, J., Genovés, A., Picornell, M., and Jansà, A.: Climatology of Mediterranean cyclones using the ERA-40 dataset, International Journal of Climatology, 31, 1596–1614, https://doi.org/10.1002/joc.2183, 2011.

Carn, S., Clarisse, L., and Prata, A. J.: Multi-decadal satellite measurements of global volcanic degassing, Journal of Volcanology and Geothermal Research, 311, 99–134, https://doi.org/10.1016/j.jvolgeores.2016.01.002, 2016.

Cavicchia, L., von Storch, H., and Gualdi, S.: A long-term climatology of medicanes, Climate dynamics, 43, 1183–1195, https://doi.org/https://doi.org/10.1007/s00382-013-1893-7, 2014.

Degeai, J.-P., Devillers, B., Dezileau, L., Oueslati, H., and Bony, G.: Major storm periods and climate forcing in the Western Mediterranean during the Late Holocene, Quaternary Science Reviews, 129, 37–56, https://doi.org/j.quascirev.2015.10.009, 2015.

Doiteau, B., Pantillon, F., Plu, M., Descamps, L., and Rieutord, T.: Systematic evaluation of the predictability of different Mediterranean cyclone categories, Weather and Climate Dynamics, 5, 1409–1427, https://doi.org/10.5194/wcd-5-1409-2024, 2024.

Ferrarin, C., Bajo, M., Benetazzo, A., Cavaleri, L., Chiggiato, J., Davison, S., Davolio, S., Lionello, P., Orlić, M., and Umgiesser, G.: Local and large-scale controls of the exceptional Venice floods of November 2019, Progress in Oceanography, 197, 102 628, https://doi.org/10.1016/j.pocean.2021.102628, 2021.

Feser, F., Barcikowska, M., Krueger, O., Schenk, F., Weisse, R., and Xia, L.: Storminess over the North Atlantic and northwestern Europe—A review, Quarterly Journal of the Royal Meteorological Society, 141, 350–382, https://doi.org/10.1002/qj.2364, 2015.

Fischer-Bruns, I., Storch, H. v., González-Rouco, J., and Zorita, E.: Modelling the variability of midlatitude storm activity on decadal to century time scales, Climate dynamics, 25, 461–476, https://doi.org/10.1007/s00382-005-0036-1, 2005.

Flaounas, E., Drobinski, P., and Bastin, S.: Dynamical downscaling of IPSL-CM5 CMIP5 historical simulations over the Mediterranean: benefits on the representation of regional surface winds and cyclogenesis, Climate dynamics, 40, 2497–2513, https://doi.org/10.1007/s00382-012-1606-7, 2013.

Flaounas, E., Kotroni, V., Lagouvardos, K., and Flaounas, I.: CycloTRACK (v1. 0)–tracking winter extratropical cyclones based on relative vorticity: sensitivity to data filtering and other relevant parameters, Geoscientific Model Development, 7, 1841–1853, https://doi.org/10.5194/gmd-7-1841-2014, 2014, 2014.

550 Flaounas, E., Lagouvardos, K., Kotroni, V., Claud, C., Delanoë, J., Flamant, C., Madonna, E., and Wernli, H.: Processes leading to heavy precipitation associated with two Mediterranean cyclones observed during the HYMEX SOP1, Quarterly Journal of the Royal Meteorological Society, 142, 275–286, https://doi.org/10.1002/qj.2618, 2015a.

Flaounas, E., Raveh-Rubin, S., Wernli, H., Drobinski, P., and Bastin, S.: The dynamical structure of intense Mediterranean cyclones, Climate Dynamics, 44, 2411–2427, https://doi.org/10.1007/s00382-014-2330-2, 2015b.

555 Flaounas, E., Kelemen, F. D., Wernli, H., Gaertner, M. A., Reale, M., Sanchez-Gomez, E., Lionello, P., Calmanti, S., Podrascanin, Z., Somot, S., et al.: Assessment of an ensemble of ocean–atmosphere coupled and uncoupled regional climate models to reproduce the climatology of Mediterranean cyclones, Climate Dynamics, 51, 1023–1040, https://doi.org/10.1007/s00382-016-3398-7, 2018.

Flaounas, E., Davolio, S., Raveh-Rubin, S., Pantillon, F., Miglietta, M. M., Gaertner, M. A., Hatzaki, M., Homar, V., Khodayar, S., Korres, G., et al.: Mediterranean cyclones: Current knowledge and open questions on dynamics, prediction, climatology and impacts, Weather and 560 Climate Dynamics, 3, 173–208, https://doi.org/10.5194/wcd-3-173-2022, 2022.

Flaounas, E., Aragão, L., Bernini, L., Dafis, S., Doiteau, B., Flocas, H., Gray, S. L., Karwat, A., Kouroutzoglou, J., Lionello, P., et al.: A composite approach to produce reference datasets for extratropical cyclone tracks: application to Mediterranean cyclones, Weather and Climate Dynamics, 4, 639–661, https://doi.org/10.5194/wcd-4-639-2023, 2023.

Fragkoulidis, G., Wirth, V., Bossmann, P., and Fink, A.: Linking Northern Hemisphere temperature extremes to Rossby wave packets, 565 Quarterly Journal of the Royal Meteorological Society, 144, 553–566, https://doi.org/10.1002/qj.3228, 2018.

Gagen, M. H., Zorita, E., McCarroll, D., Zahn, M., Young, G. H., and Robertson, I.: North Atlantic summer storm tracks over Europe dominated by internal variability over the past millennium, Nature Geoscience, 9, 630–635, https://doi.org/10.1038/ngeo2752, 2016.

Harrison, S. P., Bartlein, P., Izumi, K., Li, G., Annan, J., Hargreaves, J., Braconnot, P., and Kageyama, M.: Evaluation of CMIP5 palaeo-simulations to improve climate projections, Nature Climate Change, 5, 735–743, https://doi.org/10.1038/nclimate2649, 2015.

570 Hersbach, H., Bell, B., Berrisford, P., Hirahara, S., Horányi, A., Muñoz-Sabater, J., Nicolas, J., Peubey, C., Radu, R., Schepers, D., et al.: The ERA5 global reanalysis, Quarterly Journal of the Royal Meteorological Society, 146, 1999–2049, https://doi.org/10.1002/qj.3803, 2020.

Hochman, A., Alpert, P., Kunin, P., Rostkier-Edelstein, D., Harpaz, T., Saaroni, H., and Messori, G.: The dynamics of cyclones in the twentyfirst century: the Eastern Mediterranean as an example, Climate Dynamics, 54, 561–574, https://doi.org/10.1007/s00382-019-05017-3, 2020.

575 Hofstätter, M. and Blöschl, G.: Vb cyclones synchronized with the Arctic-/North Atlantic oscillation, Journal of Geophysical Research: Atmospheres, 124, 3259–3278, https://doi.org/10.1029/2018JD029420, 2019.

Homar, V., Jansà, A., Campins, J., Genovés, A., and Ramis, C.: Towards a systematic climatology of sensitivities of Mediterranean high impact weather: a contribution based on intense cyclones, Natural Hazards and Earth System Sciences, 7, 445–454, https://doi.org/10.5194/nhess-7-445-2007, 2007.

580 Hurrell, J. W.: Decadal trends in the North Atlantic Oscillation: Regional temperatures and precipitation, Science, 269, 676–679, https://doi.org/10.1126/science.269.5224.6, 1995.

Hurrell, J. W., Holland, M. M., Gent, P. R., Ghan, S., Kay, J. E., Kushner, P. J., Lamarque, J.-F., Large, W. G., Lawrence, D., Lindsay, K., et al.: The community earth system model: a framework for collaborative research, Bulletin of the American Meteorological Society, 94, 1339–1360, https://doi.org/10.1175/BAMS-D-12-00121.1, 2013.

Jong, R. d., Björck, S., Björkman, L., and Clemmensen, L. B.: Storminess variation during the last 6500 years as reconstructed from an ombrotrophic peat bog in Halland, southwest Sweden, Journal of Quaternary Science: Published for the Quaternary Research Association, 21, 905–919, https://doi.org/10.1002/jqs.1011, 2006.

Kageyama, M., Braconnot, P., Harrison, S. P., Haywood, A. M., Jungclaus, J., Otto-Bliesner, B. L., Peterschmitt, J.-Y., Abe-Ouchi, A., Albani, S., Bartlein, P. J., et al.: 10.22498/pages.25.3.160, Geoscientific Model Development Discussions, 11, 1033–1057, https://doi.org/10.22498/pages.25.3.160, 2018.

Kim, W. M., Blender, R., Sigl, M., Messmer, M., and Raible, C. C.: Statistical characteristics of extreme daily precipitation during 1501 BCE–1849 CE in the Community Earth System Model, Climate of the Past, 17, 2031–2053, https://doi.org/10.5194/cp-17-2031-2021, 2021.

Krug, A., Pothapakula, P. K., Primo, C., and Ahrens, B.: Heavy Vb-cyclone precipitation: a transfer entropy application showcase, Meteorologische Zeitschrift, 30, 279–284, https://doi.org/10.1127/metz/2021/1071, 2021.

Lehner, F., Joos, F., Raible, C. C., Mignot, J., Born, A., Keller, K. M., and Stocker, T. F.: Climate and carbon cycle dynamics in a CESM simulation from 850–2100 CE, Earth System Dynamics Discussions, 6, 351–406, https://doi.org/10.5194/esd-6-411-2015, 2015.

Lionello, P., Trigo, I. F., Gil, V., Liberato, M. L., Nissen, K. M., Pinto, J. G., Raible, C. C., Reale, M., Tanzarella, A., Trigo, R. M., et al.: Objective climatology of cyclones in the Mediterranean region: a consensus view among methods with different system identification and tracking criteria, Tellus A: Dynamic Meteorology and Oceanography, 68, 29 391, https://doi.org/10.3402/tellusa.v68.29391, 2016.

Lionello, P., Conte, D., and Reale, M.: The effect of cyclones crossing the Mediterranean region on sea level anomalies on the Mediterranean Sea coast, Natural Hazards and Earth System Sciences, 19, 1541–1564, https://doi.org/10.5194/nhess-19-1541-2019, 2019.

Mesinger, F. and Strickler, R. F.: Effect of mountains on Genoa cyclogeneses, Journal of the Meteorological Society of Japan. Ser. II, 60, 326–338, https://doi.org/10.2151/jmsj1965.60.1_326, 1982.

Messmer, M. and Simmonds, I.: Global analysis of cyclone-induced compound precipitation and wind extreme events, Weather and Climate Extremes, 32, 100 324, https://doi.org/10.1016/j.wace.2021.100324, 2021.

Messmer, M., Gómez-Navarro, J. J., and Raible, C. C.: Climatology of Vb cyclones, physical mechanisms and their impact on extreme precipitation over Central Europe, Earth system dynamics, 6, 541–553, https://doi.org/10.5194/esd-6-541-2015, 2015.

Montaldo, N. and Sarigu, A.: Potential links between the North Atlantic Oscillation and decreasing precipitation and runoff on a Mediterranean area, Journal of Hydrology, 553, 419–437, https://doi.org/10.1016/j.jhydrol.2017.08.018, 2017.

Mudelsee, M., Börngen, M., Tetzlaff, G., and Grünewald, U.: Extreme floods in central Europe over the past 500 years: Role of cyclone pathway "Zugstrasse Vb", Journal of Geophysical Research: Atmospheres, 109, https://doi.org/10.1029/2004JD005034, 2004.

Müller, W. A., Jungclaus, J. H., Mauritsen, T., Baehr, J., Bittner, M., Budich, R., Bunzel, F., Esch, M., Ghosh, R., Haak, H., et al.: A higher-resolution version of the max planck institute earth system model (MPI-ESM1. 2-HR), Journal of Advances in Modeling Earth Systems, 10, 1383–1413, https://doi.org/10.1029/2017MS001217, 2018.

Nissen, K., Leckebusch, G., Pinto, J. G., Renggli, D., Ulbrich, S., and Ulbrich, U.: Cyclones causing wind storms in the Mediterranean: characteristics, trends and links to large-scale patterns, Natural Hazards and Earth System Sciences, 10, 1379–1391, https://doi.org/10.5194/nhess-10-1379-2010, 2010.

Nissen, K. M., Leckebusch, G. C., Pinto, J. G., and Ulbrich, U.: Mediterranean cyclones and windstorms in a changing climate, Regional environmental change, 14, 1873–1890, https://doi.org/10.1007/s10113-012-0400-8, 2014.

Ortega, P., Lehner, F., Swingedouw, D., Masson-Delmotte, V., Raible, C. C., Casado, M., and Yiou, P.: A model-tested North Atlantic Oscillation reconstruction for the past millennium, Nature, 523, 71–74, https://doi.org/10.1038/nature14518, 2015.

PAGES Hydro2k Consortium: Comparing proxy and model estimates of hydroclimate variability and change over the Common Era, Climate of the Past, 13, 1851–1900, https://doi.org/10.5194/cp-13-1851-2017, 2017.

625   Pfahl, S. and Sprenger, M.: On the relationship between extratropical cyclone precipitation and intensity, Geophysical Research Letters, 43, 1752–1758, https://doi.org/10.1002/2016GL068018, 2016.

Pfahl, S. and Wernli, H.: Quantifying the relevance of cyclones for precipitation extremes, Journal of Climate, 25, 6770–6780, https://doi.org/10.1175/JCLI-D-11-00705.1, 2012.

Pinto, J. G. and Raible, C. C.: Past and recent changes in the North Atlantic oscillation, Wiley Interdisciplinary Reviews: Climate Change, 3,
630   79–90, https://doi.org/10.1002/wcc.150, 2012.

Portal, A., Raveh-Rubin, S., Catto, J. L., Givon, Y., and Martius, O.: Linking compound weather extremes to Mediterranean cyclones, fronts and air-streams, EGUsphere, 2024, 1–24, https://doi.org/10.5194/egusphere-2024-270, 2024.

Pouzet, P. and Maanan, M.: Temporal approaches of historical extreme storm events based on sedimentological archives, Journal of African Earth Sciences, 162, 103 710, https://doi.org/10.1016/j.jafrearsci.2019.103710, 2020.

635   Priestley, M. D., Ackerley, D., Catto, J. L., and Hodges, K. I.: Drivers of biases in the CMIP6 extratropical storm tracks. Part I: Northern Hemisphere, Journal of Climate, 36, 1451–1467, https://doi.org/10.1175/JCLI-D-20-0976.1, 2023.

Raible, C., Yoshimori, M., Stocker, T., and Casty, C.: Extreme midlatitude cyclones and their implications for precipitation and wind speed extremes in simulations of the Maunder Minimum versus present day conditions, Climate Dynamics, 28, 409–423, https://doi.org/10.1007/s00382-006-0188-7, 2007.

640   Raible, C. C., Ziv, B., Saaroni, H., and Wild, M.: Winter synoptic-scale variability over the Mediterranean Basin under future climate conditions as simulated by the ECHAM5, Climate Dynamics, 35, 473–488, https://doi.org/10.1007/s00382-009-0678-5, 2010.

Raible, C. C., Messmer, M., Lehner, F., Stocker, T. F., and Blender, R.: Extratropical cyclone statistics during the last millennium and the 21st century, Climate of the Past, 14, 1499–1514, https://doi.org/10.5194/cp-14-1499-2018, 2018.

Raible, C. C., Pinto, J. G., Ludwig, P., and Messmer, M.: A review of past changes in extratropical cyclones in the northern hemisphere and
645   what can be learned for the future, Wiley Interdisciplinary Reviews: Climate Change, 12, e680, https://doi.org/10.1002/wcc.680, 2021.

Raveh-Rubin, S. and Flaounas, E.: A dynamical link between deep Atlantic extratropical cyclones and intense Mediterranean cyclones, Atmospheric Science Letters, 18, 215–221, https://doi.org/10.1002/asl.745, 2017.

Raveh-Rubin, S. and Wernli, H.: Large-scale wind and precipitation extremes in the Mediterranean: a climatological analysis for 1979–2012, Quarterly Journal of the Royal Meteorological Society, 141, 2404–2417, https://doi.org/10.1002/qj.2531, 2015.

650   Sabatier, P., Dezileau, L., Colin, C., Briqueu, L., Bouchette, F., Martinez, P., Siani, G., Raynal, O., and Von Grafenstein, U.: 7000 years of paleostorm activity in the NW Mediterranean Sea in response to Holocene climate events, Quaternary Research, 77, 1–11, https://doi.org/10.1016/j.yqres.2011.09.002, 2012.

Schneidereit, A., Blender, R., and Fraedrich, K.: A radius–depth model for midlatitude cyclones in reanalysis data and simulations, Quarterly Journal of the Royal Meteorological Society, 136, 50–60, https://doi.org/10.1002/qj.523, 2010.

655   Seager, R., Liu, H., Henderson, N., Simpson, I., Kelley, C., Shaw, T., Kushnir, Y., and Ting, M.: Causes of increasing aridification of the Mediterranean region in response to rising greenhouse gases, Journal of Climate, 27, 4655–4676, https://doi.org/10.1175/JCLI-D-13-00446.1, 2014.

Seierstad, I., Stephenson, D., and Kvamstø, N.: How useful are teleconnection patterns for explaining variability in extratropical storminess?, Tellus A: Dynamic Meteorology and Oceanography, 59, 170–181, https://doi.org/10.1111/j.1600-0870.2007.00226.x, 2007.

660 Sigl, M., Toohey, M., McConnell, J. R., Cole-Dai, J., and Severi, M.: HolVol: Reconstructed volcanic stratospheric sulfur injections and aerosol optical depth for the Holocene (9500 BCE to 1900 CE), https://doi.org/10.1594/PANGAEA.928646, last access = 5 May 2021, 2021.

Stucki, P., Froidevaux, P., Zamuriano, M., Isotta, F. A., Messmer, M., and Martynov, A.: Simulations of the 2005, 1910, and 1876 Vb cyclones over the Alps – sensitivity to model physics and cyclonic moisture flux, Natural Hazards and Earth System Sciences, 20, 35–57,
665 https://doi.org/10.5194/nhess-20-35-2020, 2020.

Trigo, I. F.: Climatology and interannual variability of storm-tracks in the Euro-Atlantic sector: a comparison between ERA-40 and NCEP/N-CAR reanalyses, Climate Dynamics, 26, 127–143, https://doi.org/10.1007/s00382-005-0065-9, 2006.

Trigo, I. F., Davies, T. D., and Bigg, G. R.: Decline in Mediterranean rainfall caused by weakening of Mediterranean cyclones, Geophysical Research Letters, 27, 2913–2916, https://doi.org/10.1029/2000GL011526, 2000.

670 Trigo, I. F., Bigg, G. R., and Davies, T. D.: Climatology of cyclogenesis mechanisms in the Mediterranean, Monthly Weather Review, 130, 549–569, https://doi.org/10.1175/1520-0493(2002)130<0549:COCMIT>2.0.CO;2, 2002.

Vakrat, E. and Hochman, A.: Dynamical systems insights on cyclonic compound "wet" and "windy" extremes in the Eastern Mediterranean, Quarterly Journal of the Royal Meteorological Society, 149, 3593–3606, https://doi.org/10.1002/qj.4575, 2023.

van Bebber, W. J.: Die Zugstrassen der barometrischen Minima, Meteorologische Zeitschrift, 8, 361–366,
675 https://doi.org/10.1515/9783112683064-007, 1891.

Varma, V., Prange, M., Merkel, U., Kleinen, T., Lohmann, G., Pfeiffer, M., Renssen, H., Wagner, A., Wagner, S., and Schulz, M.: Holocene evolution of the Southern Hemisphere westerly winds in transient simulations with global climate models, Climate of the Past, 8, 391–402, https://doi.org/doi.org/10.5194/cp-8-391-2012, 2012.

Walz, M. A., Befort, D. J., Kirchner-Bossi, N. O., Ulbrich, U., and Leckebusch, G. C.: Modelling serial clustering and inter-
680 annual variability of European winter windstorms based on large-scale drivers, International Journal of Climatology, 38, 3044–3057, https://doi.org/10.1002/joc.5481, 2018.

Welch, B. L.: The generalization of 'STUDENT'S' problem when several different population varlances are involved, Biometrika, 34, 28–35, https://doi.org/10.2307/2332510, 1947.

Xia, L., von Storch, H., Feser, F., and Wu, J.: A study of quasi-millennial extratropical winter cyclone activity over the Southern Hemisphere,
685 Climate dynamics, 47, 2121–2138, https://doi.org/10.1007/s00382-015-2954-x, 2016.

Xoplaki, E., González-Rouco, J. F., Luterbacher, J., and Wanner, H.: Mediterranean summer air temperature variability and its connection to the large-scale atmospheric circulation and SSTs, Climate dynamics, 20, 723–739, https://doi.org/10.1007/s00382-003-0304-x, 2003.

Zappa, G., Shaffrey, L. C., and Hodges, K. I.: The ability of CMIP5 models to simulate North Atlantic extratropical cyclones, Journal of Climate, 26, 5379–5396, https://doi.org/10.1175/JCLI-D-12-00501.1, 2013.

690 Zappa, G., Masato, G., Shaffrey, L., Woollings, T., and Hodges, K.: Linking Northern Hemisphere blocking and storm track biases in the CMIP5 climate models, Geophysical Research Letters, 41, 135–139, https://doi.org/10.1002/2013GL058480, 2014.

Zscheischler, J., Westra, S., Van Den Hurk, B. J., Seneviratne, S. I., Ward, P. J., Pitman, A., AghaKouchak, A., Bresch, D. N., Leonard, M., Wahl, T., et al.: Future climate risk from compound events, Nature climate change, 8, 469–477, https://doi.org/10.1038/s41558-018-0156-3, 2018.

Table S1. Pearson correlation coefficients between the 30-year running average time series of Fig. 4.

	T850 anomalies	Cyclone frequency	Maximum cyclone-related precipitation	Maximum cyclone-related wind speed
T850 anomalies	x	-0.088	0.098	-0.224
Cyclone frequency	x	x	0.217	0.135
Maximum cyclone-related precipitation	x	x	x	0.592
Maximum cyclone-related wind speed	x	x	x	x
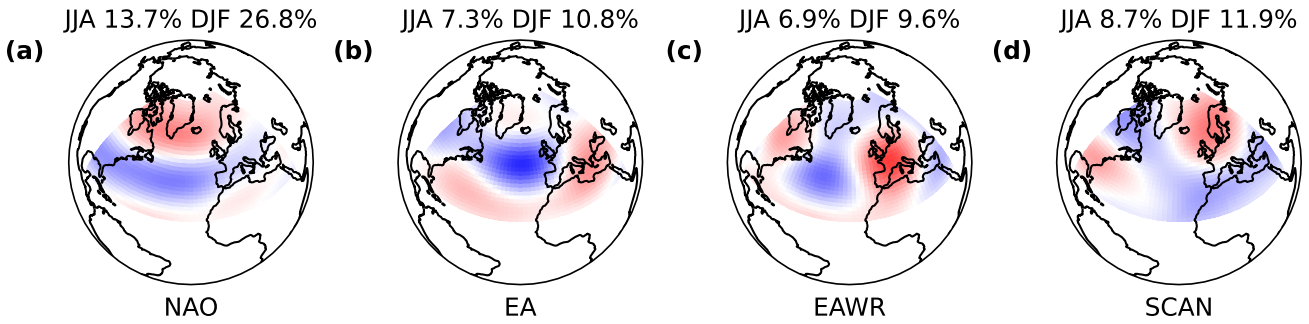
Figure S1. Shapes of EOFs that were used to compute the PCS that were correlated with cyclone frequency, cyclone-related precipitation and cyclone-related wind speed in Fig. 5 and S2. The EOF in (a) represents the NAO, (b) the EA, (c) the EAWR and (d) the SCAN pattern.

.
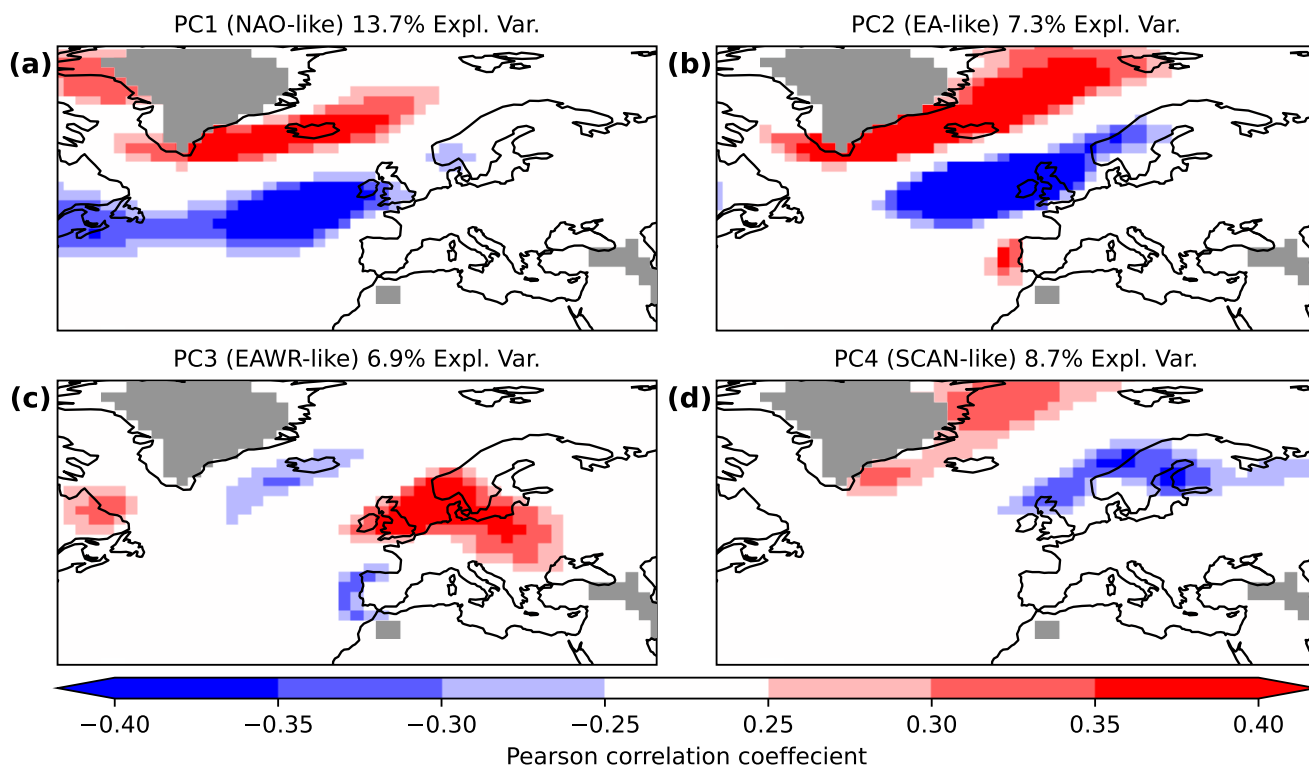
Figure S2. Same as Fig. 5, but now for JJA.

Table S2. Number of overlapping EXCs that are present in two or more extremeness rankings. CMED stands for central Mediterranean, EMED for eastern Mediterranean. The numbers outside the brackets are for DJF. The numbers within the brackets are for JJA.

	Overlap wind speed and precipitation EXCs	Overlap wind speed and compound EXCs	Overlap precipitation and compound EXCs
EXC10 CMED	0 (0)	3 (3)	3 (3)
EXC100 CMED	9 (3)	44 (44)	46 (36)
EXC1000 CMED	280 (115)	638 (461)	604 (502)
EXC10 EMED	0 (0)	3 (3)	5 (3)
EXC100 EMED	11 (3)	49 (42)	45 (37)
EXC1000 EMED	248 (114)	649 (516)	547 (372)
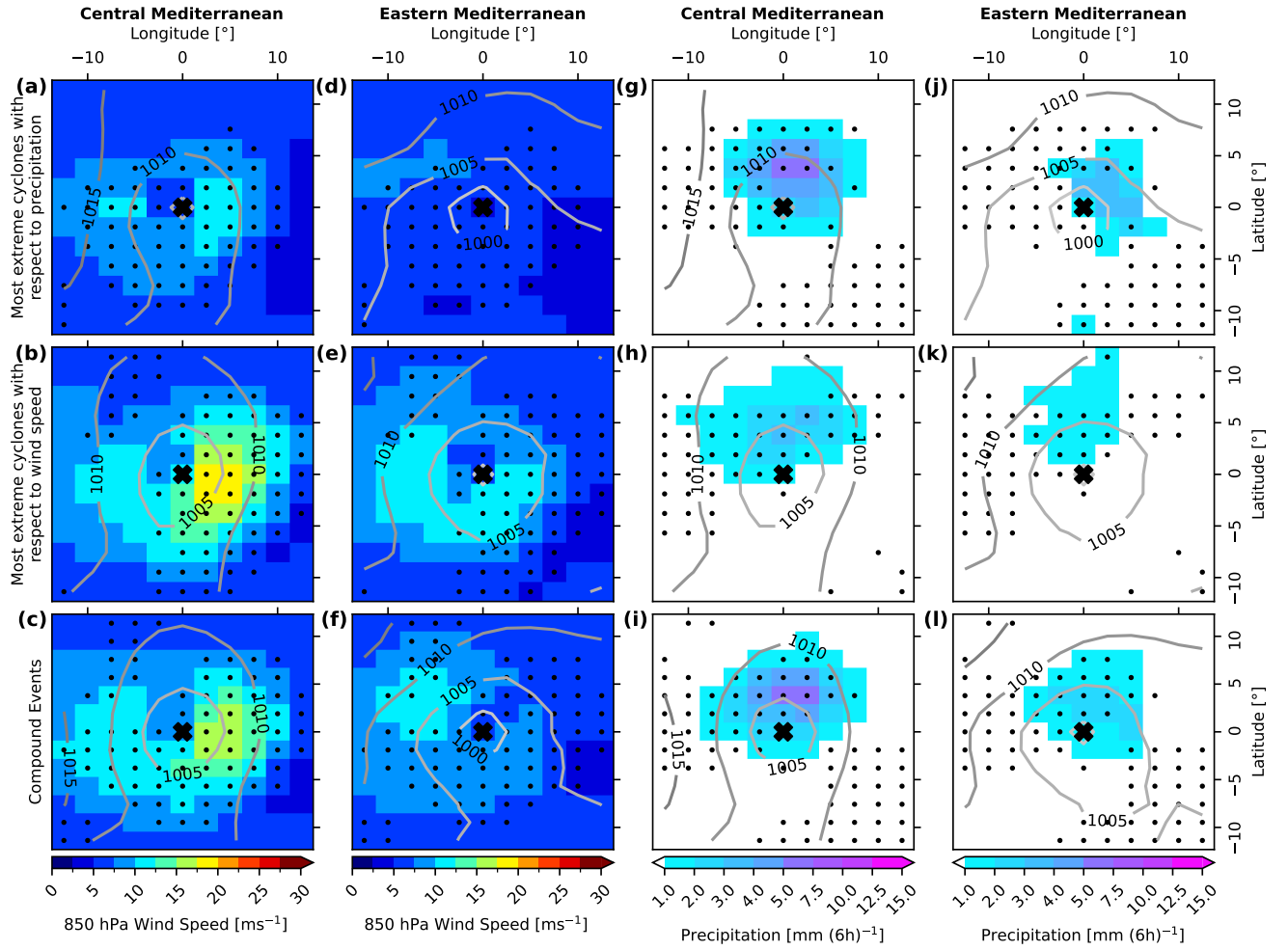
Figure S3. Same as Fig. 6, but now for JJA.
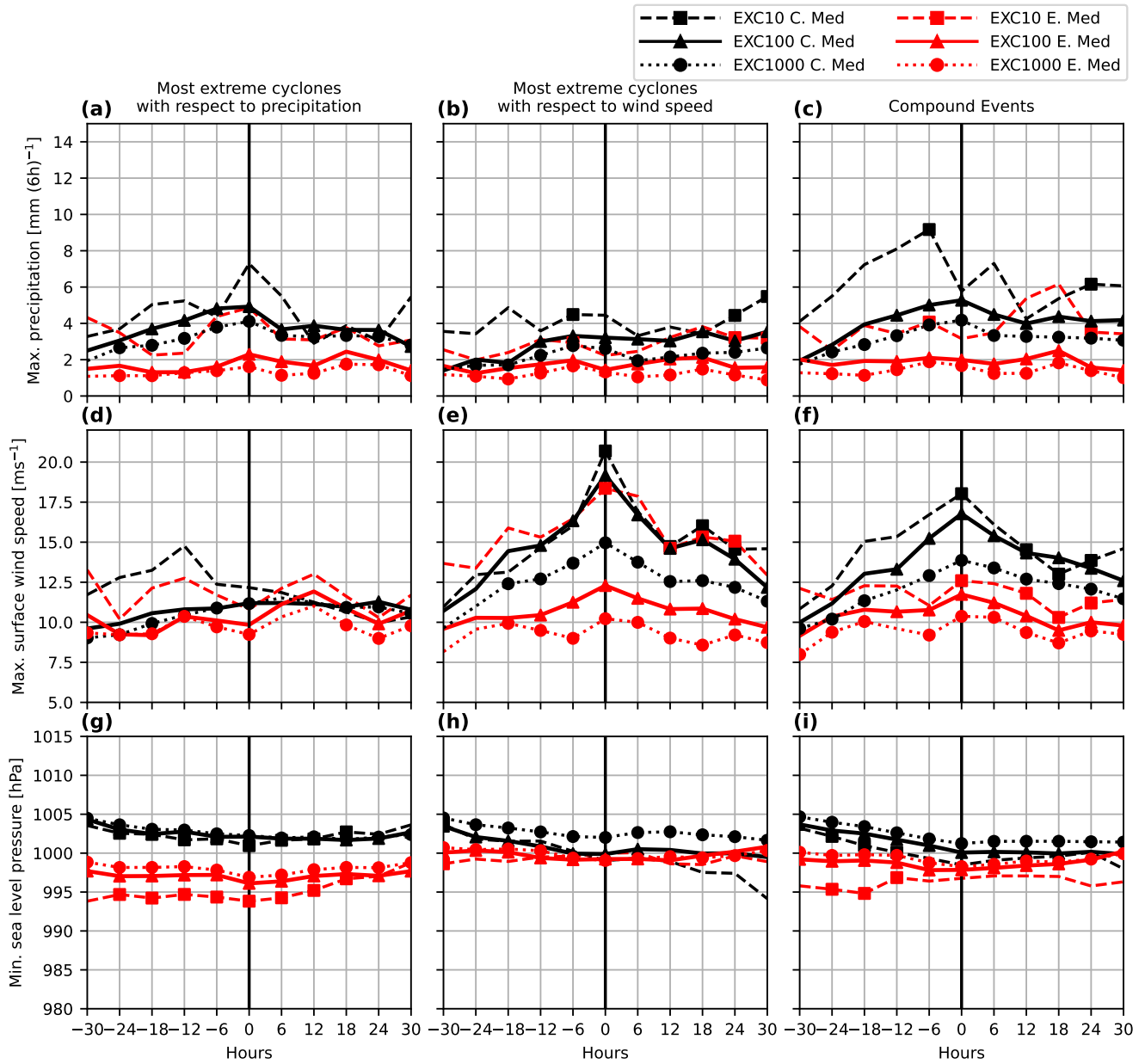
Figure S4. Same as Fig. 7, but now for JJA.

100 most extreme cyclones in the Mediterranean JJA
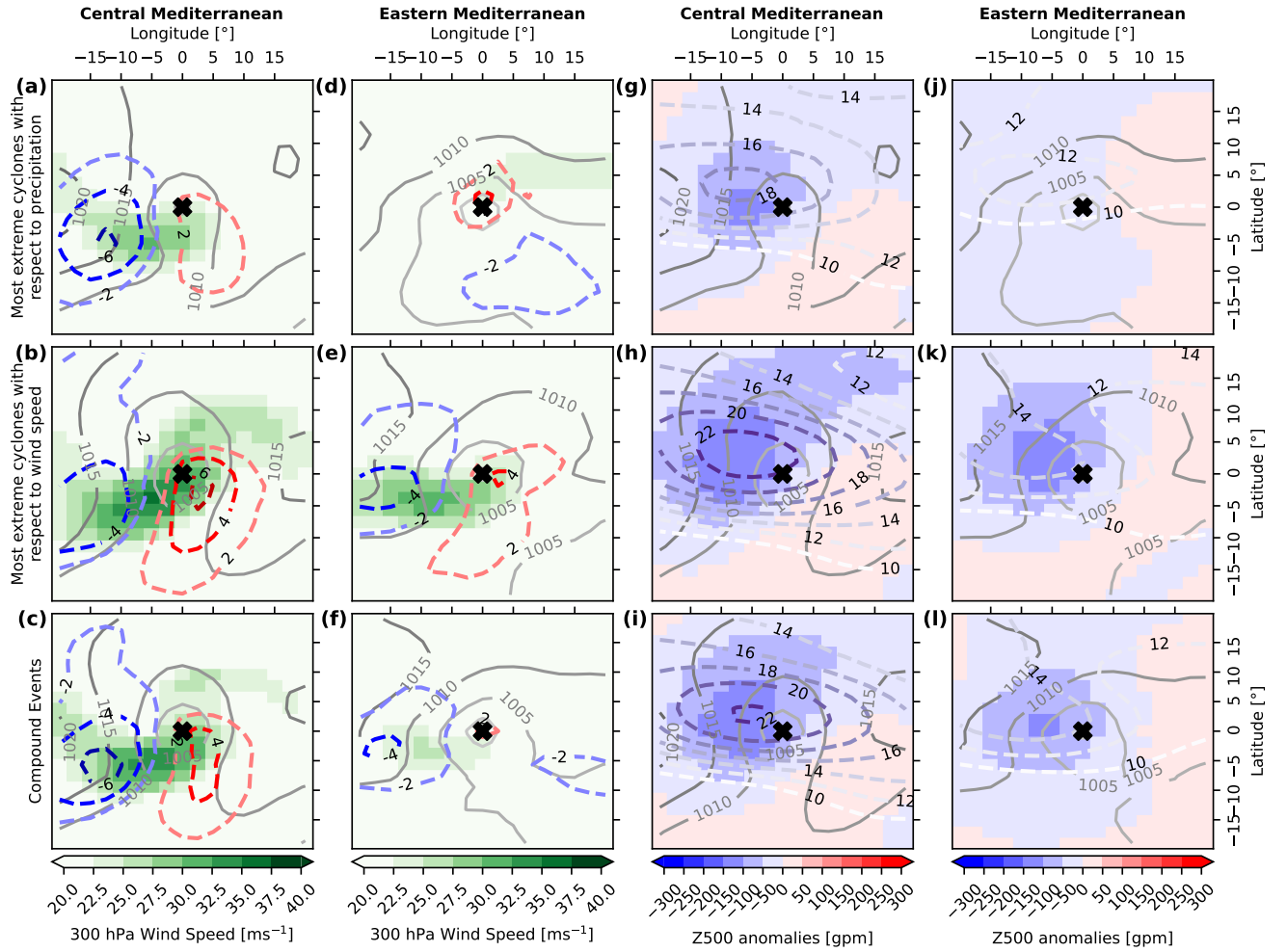
Figure S5. Same as Fig. 8, but now for JJA. Note that the colorbar for the 300 hPa wind speed is different here compared to Fig. 8.
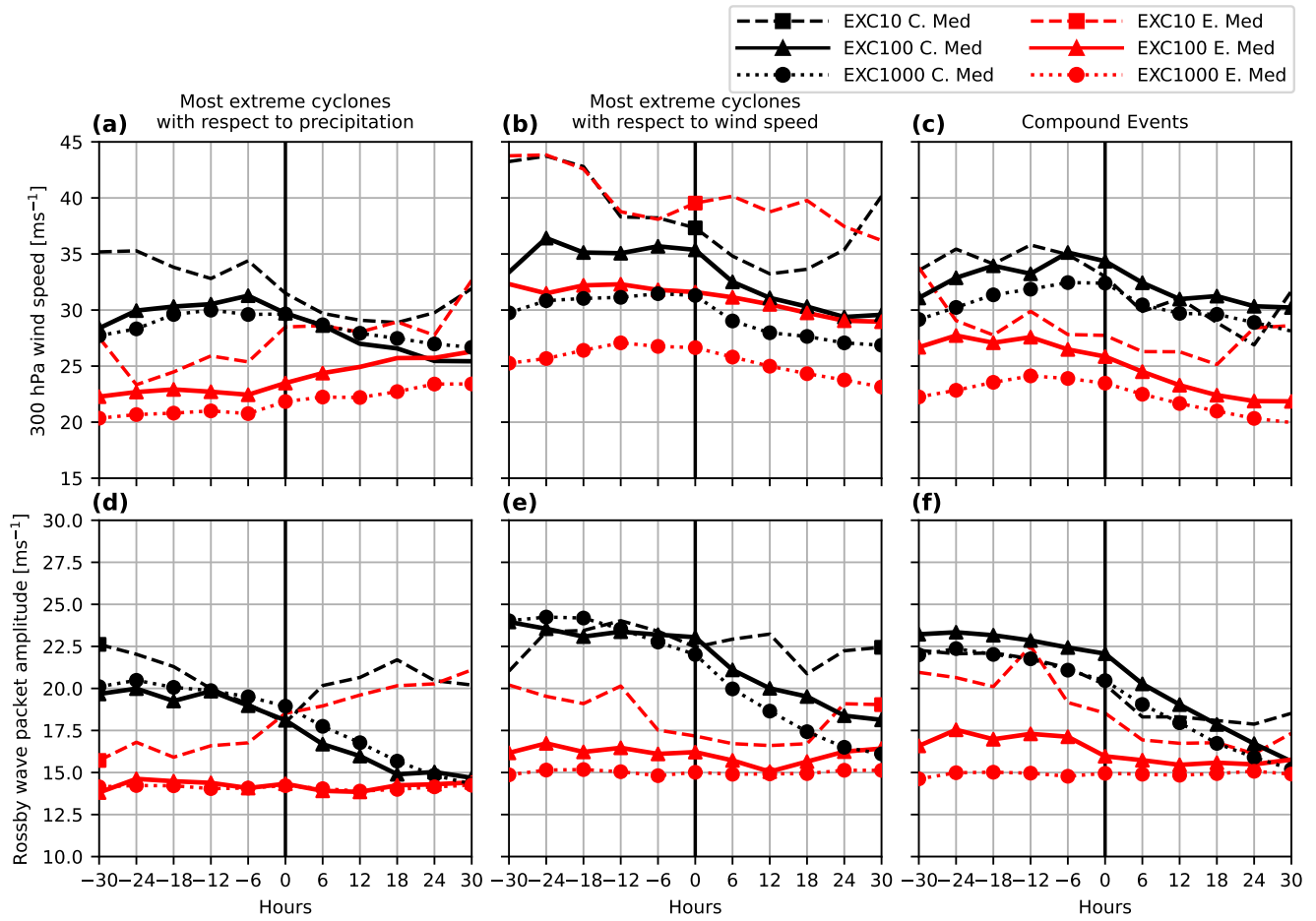
Figure S6. Same as Fig. 9, but now for JJA.